

Combining cosmological and local bounds on bimetric theory

Angelo Caravano,^{a,b} Marvin Lüben ^a, Jochen Weller ^{b,c}

^aMax-Planck-Institut für Physik (Werner-Heisenberg-Institut),
Föhringer Ring 6, 80805 Munich, Germany

^bUniversitäts-Sternwarte München, Fakultät für Physik, Ludwig-Maximilians Universität,
Scheinerstr. 1, 81679 München, Germany

^cMax Planck Institute for Extraterrestrial Physics,
Giessenbachstr. 1, 85748 Garching, Germany

E-mail: caravano@usm.lmu.de, mlueben@mpp.mpg.de, jochen.weller@usm.lmu.de

Abstract. Ghost-free bimetric theory describes two nonlinearly interacting spin-2 fields, one massive and one massless, thus extending general relativity. We confront bimetric theory with observations of Supernovae type 1a, Baryon Acoustic Oscillations and the Cosmic Microwave Background in a statistical analysis, utilising the recently proposed physical parametrisation. This directly constrains the physical parameters of the theory, such as the mass of the spin-2 field and its coupling to matter. We find that all models under consideration are in agreement with the data. Next, we compare these results to bounds from local tests of gravity. Our analysis reveals that all two- and three parameter models are observationally consistent with both cosmological and local tests of gravity. The minimal bimetric model (only β_1) is ruled out by our combined analysis.

Contents

1	Introduction	1
2	Review of bimetric theory	3
2.1	Vacuum solutions and mass eigenstates	4
2.2	FLRW solutions	5
2.3	Physical parametrisation	6
3	Bounds from cosmological observations	7
3.1	Parametrisation used for model fitting	7
3.2	Cosmological data	8
3.3	Statistical analysis and results	11
4	Bounds from local tests of gravity	15
4.1	Local tests of gravity	16
4.2	Vainshtein screening	17
4.3	Local vs. cosmological bounds	19
5	Conclusions and outlook	23
A	Details on the physical parametrisation	24
A.1	Two-parameter models	25
A.2	Three-parameter models	25
B	Vainshtein screening in static, spherically symmetric systems	27
B.1	Approximate solutions	28
B.2	Existence of Vainshtein-Yukawa branch	31

1 Introduction

In our current era of precision cosmology, cosmological tests of gravity with remarkable accuracy become available. On the one hand, the direct detection of gravitational waves by the LIGO/Virgo collaboration [1] has confirmed some of the most fundamental predictions of general relativity – gravitational waves [2]. Moreover, the joint detection of gravitational waves with their electromagnetic counterpart [3] show that gravitational waves indeed travel at the speed of light to large precision [4]. On the other hand, measurements of the cosmic microwave background [5, 6] and local observables [7–10] challenge the standard model of cosmology. In fact, the discrepancy between the inferred value for the Hubble parameter today (H_0) from early and late-time measurements represents a substantial tension [11]. From a theoretical perspective, the cosmological constant problems remain unsolved [12, 13]. In addition, concerns about the quantum consistency of a positive cosmological constant have been raised, in the context of quantum breaking [14–17] and the swampland¹ [19–22].

Therefore, it is worth investigating theories beyond the standard model of cosmology, which modify the gravitational theory or replace the cosmological constant by some dark energy [23]. To modify gravity, one has to break one of the axioms of Lovelock’s theorem [24]. A particularly simple possibility is to add new degrees of freedom to the gravitational sector. The resulting scalar-tensor [25, 26] and vector-tensor [27, 28] theories are already tightly constrained by gravitational wave observations and forced into their simplest forms [29–32]. Also massive gravity [33, 34] is tightly constrained observationally [35]. Contrarily, bimetric theory [36] remains mostly unconstrained by the determination of the propagation speed of gravitational waves [37, 38]. In the present paper, we will further investigate the observational viability of the latter theory.

¹For a critical perspective on the de Sitter conjectures and the cosmological implications, see e.g. [18].

Historically, the question of whether the graviton can have a finite mass goes back to Fierz and Pauli, who presented a linear theory of a massive graviton in [39]. However, this theory failed even basic solar-system tests of gravity due to the van Dam-Veltman-Zakharov (vDVZ) discontinuity [40, 41]. Shortly after, Vainshtein argued that nonlinear terms might cure the discontinuity and render a nonlinear theory of a massive graviton observationally viable [42]. However, Boulware and Deser argued that a fully nonlinear theory of a massive graviton will inevitably introduce an additional degree of freedom (d.o.f.) with negative norm². Rather recently, de Rham, Gabadadze and Tolley identified a loop-hole in the argument, which led to the construction of a fully nonlinear and ghost-free theory of massive gravity [33, 34, 46]³. The construction of a nonlinear theory for a massive graviton requires the introduction of a reference metric, which is kept fixed. A natural extension is to promote this fixed reference metric to be dynamical, which leads to ghost-free bimetric theory [36].

While massive gravity describes a single massive graviton, bimetric theory contains a massless and a massive spin-2 field [36]. This yields distinct phenomenological features. The mass m_{FP} of a single massive graviton is tightly constrained. While gravitational wave observations provide the upper bound of $m_{\text{FP}} \lesssim 10^{-22}$ eV [32], the most stringent constraints come from the solar system with $m_{\text{FP}} \lesssim 10^{-33}$ eV [35]. Moreover, massive gravity does not give rise to viable homogenous and isotropic cosmological solutions [53–56]. Reviews on theoretical and phenomenological aspects of massive gravity can be found in [35, 57, 58].

Contrarily, bimetric theory has a viable and rich phenomenology. In the context of cosmology, the theory allows for homogeneous and isotropic cosmological solutions with late-time de Sitter attractor. The (self-)interactions of the massive and massless spin-2 fields give rise to dynamical dark energy, even in the absence of vacuum energy, i.e. so-called self-accelerating solutions [59–67]. Bimetric theory can alleviate the H_0 -tension if the spin-2 mass is of the order of the Hubble constant [68, 69]. Cosmological perturbations and cosmic structure formation remain challenging due to the gradient instability at early times [65, 70–80], which might be cured by nonlinear terms in analogy to the Vainshtein mechanism [69, 81, 82]. The theory contains the massive spin-2 field as dark-matter candidate [83–86].

Spherically symmetric solutions [87] have been confronted with observations on galaxy cluster [88], galactic [88–90], and solar system scales [90–92]. The nonlinear Vainshtein mechanism suppresses modifications in the gravitational sector on small scales [90, 93]. Going further, gravitational waves were studied in [78, 94–104], with an application to binary mergers [37, 38]. Summarising, bimetric theory is in agreement with the current corresponding observational bounds and even leads to possibly detectable effects, but it is not clear, whether the theory is consistent with all theoretical and observational constraints simultaneously.

To consistently combine the various observational and theoretical constraints on the parameter space, a new parametrisation of bimetric solutions was developed in [105]. The idea is to formulate solutions in terms of the following physical parameters: mass of the spin-2 field, its coupling constant to ordinary matter and the effective asymptotic cosmological constant. The procedure automatically yields theoretical constraints that ensure a viable cosmic expansion history, i.e. real-valued, non-singular and devoid of the Higuchi ghost.

In this paper, we extend the analysis of [105] to test bimetric cosmology against data from Supernovae type 1a (SN1a), Baryon Acoustic Oscillations (BAOs) and the Cosmic Microwave Background (CMB). While bimetric theory has been tested against these data sets beforehand [60, 64, 67, 68, 106, 107], here we directly constrain the physical parameters. We restrict our analysis to all theoretically viable bimetric models with up to three free interaction parameters⁴. In addition, we allow for non-zero spatial curvature in the statistical analysis.

²This additional degree of freedom is commonly referred to as Boulware-Deser ghost, which represents a Laplacian instability [43–45]. Such an instability spoils unitarity and renders the theory ill-defined.

³Since then, the ghost-freedom of massive gravity and its extensions was confirmed in a series of papers utilising various methods, see e.g. [47–51]. For a pedagogical paper on how to consistently count the number of propagating degrees of freedom in first-order field theories, see [52].

⁴To be more precise, we consider all models with up to three free parameters β_n . Strictly speaking, the parameters $\beta_{1,2,3}$ parametrise interactions, while the parameters $\beta_{0,4}$ parametrise vacuum energy.

Next, we compare the cosmological bounds to bounds from local tests of gravity. We use tests of the Newtonian gravitational potential from laboratory to planetary scale as summarised in [108–111]. The Yukawa parametrisation, where the gravitational potential is written as a superposition of the usual $1/r$ -term and a Yukawa-term, is appropriate for our purposes. We use the existing bounds to constrain the physical parameters of bimetric theory. We add further bounds from tests of the scalar curvature, i.e. measurements of the deflection and time delay of light [91, 112, 113].

The aforementioned frameworks are appropriate only in regimes without Vainshtein screening. In screened spacetime regions these bounds are not trustworthy, because deviations from general relativity (GR) are suppressed. However, only a subregion of the full bimetric parameter space supports Vainshtein screening. In this paper, we relate the bounds of [90, 93], which ensure a working Vainshtein mechanism, to the physical parameters and identify the region of the physical parameter space that supports screening. We will see that the Vainshtein mechanism does not affect the observational bounds from local tests of gravity, such that these are directly applicable. Summarising, we consistently combine for the first time these observational and theoretical constraints from cosmology and local tests of gravity with each other.

This paper is organised as follows. We start with a brief summary of bimetric theory, the cosmological solutions and the physical parameters in section 2. We proceed with the statistical analysis using cosmological data in section 3. In section 4, we discuss the bounds from local tests of gravity and the Vainshtein screening, which we confront with the cosmological constraints. We summarise our analysis and conclude in section 5.

2 Review of bimetric theory

In this section we briefly discuss bimetric theory, its mass spectrum, cosmological solutions and the physical parametrisation. For a thorough introduction to the field we refer to [114].

The construction of a nonlinear mass term involves two metric tensors, which we call $g_{\mu\nu}$ and $f_{\mu\nu}$. The action of ghost-free bimetric theory for these metrics reads [33, 34, 36, 46, 115]

$$S = m_g^2 \int d^4x \left[\sqrt{-g} R^g + \alpha^2 \sqrt{-f} R^f - 2\mathcal{U}(\sqrt{g^{-1}f}) \right] + \int d^4x \sqrt{-g} \mathcal{L}_m(g, \Phi) \quad (2.1)$$

where R^g and R^f are the Ricci scalars of $g_{\mu\nu}$ and $f_{\mu\nu}$, resp. The parameter m_g is the Planck mass of $g_{\mu\nu}$ and α is the Planck mass of $f_{\mu\nu}$ normalised to m_g . The ghost-free bimetric potential \mathcal{U} is defined in terms of the square-root matrix $S = \sqrt{g^{-1}f}$ and given by⁵

$$\mathcal{U}(\sqrt{g^{-1}f}) = \sum_{n=0}^4 \beta_n e_n(\sqrt{g^{-1}f}). \quad (2.2)$$

Here, β_n are real parameters with mass dimension two in our parametrisation. The functions e_n are the elementary symmetric polynomials [115]. Matter fields are collectively denoted by Φ , which minimally couple⁶ to the metric $g_{\mu\nu}$ via the matter Lagrangian \mathcal{L}_m . Hence, $g_{\mu\nu}$ is the physical metric that defines the geometry in which the matter fields propagate.

Varying the action with respect to $g^{\mu\nu}$ and $f^{\mu\nu}$ yields the modified Einstein equations

$$G_{\mu\nu}^g + \mathcal{U}_{\mu\nu}^g = \frac{1}{m_g^2} T_{\mu\nu}, \quad G_{\mu\nu}^f + \alpha^{-2} \mathcal{U}_{\mu\nu}^f = 0, \quad (2.3)$$

where $G_{\mu\nu}^{g,f}$ are the Einstein tensors of $g_{\mu\nu}$ and $f_{\mu\nu}$, resp. The terms coming from the variation of the bimetric potential are given by

$$\mathcal{U}_{\mu\nu}^g = \sum_{n=0}^3 (-1)^n \beta_n g_{\mu\lambda} Y_{(n)\nu}^\lambda(S), \quad \mathcal{U}_{\mu\nu}^f = \sum_{n=0}^3 (-1)^n \beta_{4-n} f_{\mu\lambda} Y_{(n)\nu}^\lambda(S^{-1}) \quad (2.4)$$

⁵Note that bimetric theory is well-defined only if both metrics have a common time direction [116].

⁶This setup is referred to singly-coupled bimetric theory. More general ghost-free matter couplings exist in bimetric theory [117–122].

where the matrices $Y_{(n)\nu}^\lambda$ are given in, e.g. [115]. Since matter couples to the physical metric $g_{\mu\nu}$, the matter stress-energy tensor is given by

$$T_{\mu\nu} = \frac{-2}{\sqrt{-g}} \frac{\delta \sqrt{-g} \mathcal{L}_m}{\delta g^{\mu\nu}}. \quad (2.5)$$

If the matter sector is invariant under diffeomorphisms, the stress-energy tensor of matter is conserved,

$$\nabla^\mu T_{\mu\nu} = 0, \quad (2.6)$$

where ∇_μ is the covariant derivative compatible with $g_{\mu\nu}$. The Bianchi identity, $\nabla^\mu G_{\mu\nu}^g = 0$, then yields the so-called Bianchi constraint,

$$\nabla^\mu \mathcal{U}_{\mu\nu}^g = 0. \quad (2.7)$$

The Bianchi identity in the $f_{\mu\nu}$ -sector yields another Bianchi constraint, which however coincides with eq. (2.7) by diffeomorphism invariance.

2.1 Vacuum solutions and mass eigenstates

Before moving to cosmology, we briefly review an important class of solutions in bimetric theory [36, 123]. Let both metric tensors be proportional as $f_{\mu\nu} = c^2 g_{\mu\nu}$ with conformal factor c . This ansatz is a solution to the modified Einstein equations only in vacuum, i.e. for $T_{\mu\nu} = 0$. The Bianchi constraint (2.7) implies that c is a constant. Upon this ansatz, the modified Einstein equations (2.3) simplify to

$$G^g + \Lambda_g g_{\mu\nu} = 0, \quad G_{\mu\nu}^f + c^{-2} \Lambda_f f_{\mu\nu} = 0, \quad (2.8)$$

where the effective cosmological constants are given in terms of the bimetric parameters as

$$\Lambda_g = \beta_0 + 3\beta_1 c + 3\beta_2 c^2 + \beta_3 c^3, \quad \Lambda_f = \frac{1}{\alpha^2 c^2} (\beta_1 c + 3\beta_2 c^2 + \beta_3 c^3 + \beta_4 c^4). \quad (2.9)$$

Subtracting both equations in (2.8) and using that both metrics are conformally related yields $\Lambda_g = \Lambda_f \equiv \Lambda$, or in terms of the bimetric parameters

$$\alpha^2 \beta_3 c^4 + (3\alpha^2 \beta_2 - \beta_4) c^3 + 3(\alpha^2 \beta_1 - \beta_3) c^2 + (\alpha^2 \beta_0 - \beta_3) c - \beta_1 = 0. \quad (2.10)$$

This is a polynomial in c of degree 4. Hence, there are up to four real-valued solutions for c in terms of the bimetric parameters α and β_n , each corresponds to a vacuum solution.

Bimetric theory has a well-defined mass spectrum around proportional solutions. Let us perturb the metrics around the background $\bar{g}_{\mu\nu}$ as

$$g_{\mu\nu} = \bar{g}_{\mu\nu} + \frac{1}{m_g} \delta g_{\mu\nu}, \quad f_{\mu\nu} = c^2 \bar{g}_{\mu\nu} + \frac{c}{\alpha m_g} \delta f_{\mu\nu}, \quad (2.11)$$

where $\delta g_{\mu\nu} \ll m_g$ and $\delta f_{\mu\nu} \ll \alpha m_g$ are small fluctuations around the proportional background $\bar{f}_{\mu\nu} = c^2 \bar{g}_{\mu\nu}$. The mass eigenstates are linear superpositions of the metric fluctuations. The spectrum contains a massless mode, $\delta G_{\mu\nu}$, and a massive mode, $\delta M_{\mu\nu}$, with Fierz-Pauli mass⁷

$$m_{\text{FP}}^2 = \left(1 + \frac{1}{\alpha^2 c^2} \right) c (\beta_1 + 2\beta_2 c + \beta_3 c^2). \quad (2.12)$$

We can express the metric fluctuations in terms of the mass eigenstates as

$$\delta g_{\mu\nu} = \frac{1}{\sqrt{1 + \bar{\alpha}^2}} (\delta G_{\mu\nu} - \bar{\alpha} \delta M_{\mu\nu}), \quad \delta f_{\mu\nu} = \frac{1}{\sqrt{1 + \bar{\alpha}^2}} (\delta M_{\mu\nu} + \bar{\alpha} \delta G_{\mu\nu}). \quad (2.13)$$

Here, we defined $\bar{\alpha} = \alpha c$ that parametrises the mixing of the massless and the massive mode in the metric fluctuations. From here we can already identify the GR and massive gravity limit of bimetric theory [80, 92]. The GR-limit is $\bar{\alpha} \rightarrow 0$ because then the fluctuation of $g_{\mu\nu}$ is aligned with the massless mode while the fluctuation of $f_{\mu\nu}$ is aligned with the massive mode. In the opposite limit $\bar{\alpha} \rightarrow \infty$ bimetric theory approaches massive gravity as then $\delta g_{\mu\nu}$ is aligned with the massive mode while $\delta f_{\mu\nu}$ coincides with the massless mode.

⁷The mass term of $\delta M_{\mu\nu}$ has the Fierz-Pauli structure [39].

2.2 FLRW solutions

Assuming homogeneity and isotropy according to the cosmological principle, both metric can be cast into the Friedmann-Lemaître-Robertson-Walker (FLRW) form [59–61],

$$ds_g^2 = -dt^2 + a^2 \left(\frac{dr^2}{1 - kr^2} + r^2 d\Omega^2 \right), \quad ds_f^2 = -X^2 dt^2 + b^2 \left(\frac{dr^2}{1 - kr^2} + r^2 d\Omega^2 \right), \quad (2.14)$$

where a and b are the scale factors of $g_{\mu\nu}$ and $f_{\mu\nu}$, respectively, while X is the lapse of $f_{\mu\nu}$. These metric functions depend on time t only. Further, k is the spatial curvature, which must be common to both metrics [124]. In this coordinate system, $k < 0$, $k = 0$, $k > 0$ describes a closed, flat, or open universe, resp. Let us define the Hubble rates and the scale factor ratio as

$$H = \frac{\dot{a}}{a}, \quad H_f = \frac{\dot{b}}{Xb}, \quad y = \frac{b}{a}, \quad (2.15)$$

where dot denotes derivative with respect to cosmic time t .

On the bidiagonal FLRW ansatz (2.14), the Bianchi constraint (2.7) simplifies to

$$(\dot{b} - X\dot{a})(\beta_1 + 2\beta_2 y + \beta_3 y^2) = 0. \quad (2.16)$$

This equation has two branches of solution. We use the so-called dynamical branch solution with $X = \dot{b}/\dot{a}$ for the remainder of this paper⁸. Then the Hubble rates are related as $H = yH_f$.

We take the matter source to be a perfect fluid with stress-energy tensor

$$T^{\mu\nu} = (\rho + p)u^\mu u^\nu + p g^{\mu\nu} \quad (2.17)$$

with energy density ρ , pressure p and u^μ the 4-velocity of the fluid. We split energy density and pressure into a non-relativistic and a relativistic part as $\rho = \rho_m + \rho_r$ and $p = p_m + p_r$, resp. The subscript m refers to non-relativistic matter, while the subscript r refers to radiation. The conservation of energy-momentum (2.6) leads to the continuity equation

$$\dot{\rho}_i = -3H(1 + w_i)\rho_i, \quad i = m, r, \quad (2.18)$$

with $w_i = p_i/\rho_i$ the equation of state. Therefore, the energy density of matter and radiation evolve with the scale factor a of the physical metric as in standard cosmology. To be explicit, the continuity equation is solved by

$$\rho_i = \rho_{i,0} a^{-3(1+w_i)}, \quad (2.19)$$

unless $w_i = -1$, with the integration constants chosen such that $\rho_{i,0} = \rho_i(1)$, where $a = 1$ corresponds to the present time. Radiation has an equation of state of $w_r = 1/3$ while for matter $w_m = 0$.

The time-time component of the two modified Einstein equations (2.3) become

$$3H^2 + 3\frac{k}{a^2} = \frac{1}{m_g^2} (\rho_{de} + \rho_m + \rho_r), \quad 3H^2 + 3\frac{k}{a^2} = \frac{1}{m_g^2} \rho_{pot}. \quad (2.20)$$

Here we defined the energy density of the dynamical dark energy induced by the bimetric potential as

$$\frac{\rho_{de}}{m_g^2} = \beta_0 + 3\beta_1 y + 3\beta_2 y^2 + \beta_3 y^3 \quad (2.21)$$

with the time-dependent function y . The Friedmann equation of $f_{\mu\nu}$ is sourced by potential energy only with energy density

$$\frac{\rho_{pot}}{m_g^2} = \frac{1}{\alpha^2} \left(\frac{\beta_1}{y} + 3\beta_2 + 3\beta_3 y + \beta_4 y^2 \right). \quad (2.22)$$

⁸On the other branch of solutions, referred to as algebraic, the scale factor ratio is forced to be constant, $y = \text{const}$. Since this solution is found to be pathological [70, 125], we focus on the dynamical branch solution.

Interpreting the effect of spatial curvature as an energy source, we can define the energy density

$$\rho_k = -3m_g^2 k a^{-2}. \quad (2.23)$$

Then, the Friedmann eq. (2.20) of $g_{\mu\nu}$ can be written as

$$3H^2 = \frac{1}{m_g^2} (\rho_{de} + \rho_k + \rho_m + \rho_r). \quad (2.24)$$

It remains to determine the time-evolution of ρ_{de} , which in general cannot be written as a polynomial in $1/a$. Subtracting the the Friedmann equations in (2.20) yields

$$\alpha^2 \beta_3 y^4 + (3\alpha^2 \beta_2 - \beta_4) y^3 + 3(\alpha^2 \beta_1 - \beta_3) y^2 + \left(\alpha^2 \beta_0 - 3\beta_2 + \alpha^2 \frac{\rho_m + \rho_r}{m_g^2} \right) y - \beta_1 = 0. \quad (2.25)$$

This equation determines the time evolution of y in terms of the time evolution of the matter energy densities. It is a quartic polynomial in y , hence there are up to four real-valued solutions with different time evolutions of y . Following [60, 67], we can distinguish three classes of solutions by inspecting the early-time behavior, for which the energy densities classically diverge:

- *Finite branch.* The first possible early-time behavior is that y approaches zero so as to compensate the diverging value of the energy density in the linear piece of the polynomial (2.25). Hence, during early times the scale factor ratio can be approximated as $y \sim m_g^2 \beta_1 / (\alpha^2 \rho)$. Existence of the finite branch requires $\beta_1 > 0$. The scale factor ratio monotonically increases in time. In the asymptotic future, the energy densities vanish and y approaches a constant value c , which corresponds to the lowest-lying, strictly positive root of eq. (2.10) [105]. For positive matter and radiation energy densities, this branch of solution satisfies the cosmological stability bound, a generalization of the Higuchi bound to FLRW spacetime [79, 126].
- *Infinite branch.* The alternative is that y is large as the energy densities are large. Then, at early times, the evolution can be approximated as $y^3 \sim -\rho / (m_g^2 \beta_3)$. This reveals that the infinite branch exists only if $\beta_3 < 0$. The scale factor ratio monotonically decreases in time. In the asymptotic future, when the energy densities vanish, y approaches the highest lying, strictly positive root of eq. (2.10) [105]. This branch, however, inevitably violates the cosmological stability bound and is therefore not a physical solution [79, 126].

Due to the high degree of the polynomial (2.25), there are further *exotic branches* of solutions, which however do not give rise to a viable expansion history [79]. Therefore, we pick out the finite branch solution in section 3. The scale factor ratio then satisfies $0 < y < c$ [79, 105].

Let us pause for a moment and summarise. The bimetric potential contributes a dynamical dark energy to the Friedmann equation in the form of ρ_{de} , which depends on the scale factor ratio y . Since y approaches a constant value c in the asymptotic future, ρ_{de} approximates the effect of a cosmological constant at late times. We have identified two possible time evolutions for y yielding a consistent expansion history. Out of these, only the finite branch solution satisfies the cosmological stability bound. Therefore, y decreases when looking back in time, implying that also ρ_{de} decreases. In other words, the (self-)interactions of the massive and massless spin-2 field are dynamically increasing as time proceeds. Hence, the (self-)interaction energy is necessarily phantom or negative [69, 79].

2.3 Physical parametrisation

The solutions presented thus far are parametrised in terms of the Planck mass ratio α and the interaction parameters β_n . Vacuum solutions are labeled by c that are the roots of eq. (2.10). The bimetric action and hence the equations of motion are invariant under a rescaling of these parameters implying that one of them is redundant.

In [105] a parametrisation that is invariant under this rescaling is proposed and worked out. It relies on the following physical parameters: the mass m_{FP} of the spin-2 field, its coupling to matter $\bar{\alpha}$, and the effective cosmological constant Λ . The hence baptised physical parametrisation allows

to unambiguously combine various theoretical and observational bounds on the parameter space of bimetric theory.

Let us give more detail on the physical parametrisation and on the already inferred theoretical consistency bounds. Since there are up to four real-valued roots c of eq. (2.10), the relation between the physical and interaction parameters is not unique. However, a vacuum solution and the cosmic expansion history are well-defined only under the following conditions:

- *Consistent de Sitter vacuum.* Without loss of generality we restrict ourselves to roots with $c > 0$ ⁹. We impose that the mass of the spin-2 field is positive, $m_{\text{FP}} > 0$, and we restrict ourselves to de Sitter vacua, $\Lambda > 0$. For a massive spin-2 field propagating in de Sitter space, unitarity forbids the mass to be arbitrarily small. Instead, the Higuchi bound [127]

$$3m_{\text{FP}}^2 > 2\Lambda \quad (2.26)$$

has to be satisfied. If the bound is violated, the helicity-0 mode of the massive spin-2 field has a negative norm (Higuchi ghost).

- *Consistent asymptotic future.* The cosmic expansion has to approach a consistent de Sitter vacuum in the asymptotic future. Since only the finite branch solution to the Friedmann equations is physical, the scale factor ratio satisfies $0 < y < c$. Hence, the lowest-lying strictly positive root of eq. (2.10) as the unique physical vacuum solution. Identifying the asymptotic future of the cosmic expansion history with the physical vacuum solution implies further, model-dependent conditions on the bimetric parameters.
- *Consistent cosmic expansion history.* The consistency of the early universe for a cosmic expansion history on the finite branch requires [67]

$$\beta_1 > 0, \quad (2.27)$$

as can be seen from eq. (2.20). Otherwise $H^2 \leq 0$ during early times.

These restrictions imply a unique relation between the physical and interaction parameters. The details for all bimetric models with up to three non-vanishing interaction parameters are worked out in Ref. [105]. For completeness, we summarise the explicit expressions in table 4. Using the physical parametrisation, in section 3 we compute bounds from cosmological observations.

3 Bounds from cosmological observations

We now compare bimetric theory to cosmological observables. We restrict ourselves to background observables that constrain the Hubble rate at different redshifts. In particular, we use Supernovae type Ia, Baryon Acoustic Oscillations and the first peak of the oscillations in the Cosmic Microwave Background, which we discuss in greater detail in section 3.2.

Measurements of perturbative quantities are not included because of the aforementioned gradient instability in the scalar sector [65, 70–80]. The scale at which the gradient instability kicks in is set by the spin-2 mass [69]. Taking nonlinearities into account possibly stabilises the perturbations at early times [81, 82, 128]. However, a framework to study cosmological phenomena on the perturbative level within bimetric theory is still pending.

3.1 Parametrisation used for model fitting

We have already explained how to get the time-evolution of the scale factor ratio y , the time evolution of ρ_{de} and hence the time evolution of H . To ease these computations, it is convenient to introduce the energy density parameters

$$\Omega_i = \frac{\rho_i}{3m_{\text{g}}^2 H^2}, \quad i = \{\text{de}, \text{k}, \text{m}, \text{b}, \text{r}, \gamma\}. \quad (3.1)$$

⁹Solutions with $c < 0$ can be mapped onto solutions with $c > 0$ because the equations of motion are invariant under the combined rescaling $c \rightarrow -c$, $\beta_n \rightarrow (-1)^n \beta_n$.

The Friedmann equation (2.24) can then be written in the compact form

$$\Omega_{\text{de}} + \Omega_{\text{k}} + \Omega_{\text{m}} + \Omega_{\text{r}} = 1. \quad (3.2)$$

Evaluating this equation at present times yields the following relation between the parameters as

$$\Omega_{\text{de}0} + \Omega_{\text{k}0} + \Omega_{\text{m}0} + \Omega_{\text{r}0} = 1. \quad (3.3)$$

We choose to express the parameter $\Omega_{\text{m}0}$ in terms of the other parameters in our statistical analysis. In order to compute Ω_{de} , we introduce the following constant parameters:

$$B_n = \frac{\alpha^{-n} \beta_n}{3H_0^2}, \quad \Omega_{\text{FP}} = \frac{m_{\text{FP}}^2}{3H_0^2}, \quad \Omega_{\Lambda} = \frac{\Lambda}{3H_0^2}. \quad (3.4)$$

The relations between B_n and the physical parameters $\bar{\alpha}$, Ω_{FP} , and Ω_{Λ} are presented in appendix A as derived in [105]. Note that B_n is rescaling-invariant and hence observable. Further, in analogy to the definition of $\bar{\alpha}$, we define the rescaled scale factor ratio as $\bar{y} = \alpha y$. To be explicit, the energy density parameter of the induced dynamical dark energy is given as

$$E^2 \Omega_{\text{de}} = B_0 + 3B_1 \bar{y} + 3B_2 \bar{y}^2 + B_3 \bar{y}^3, \quad (3.5)$$

where $E = H/H_0$ is the normalised Hubble rate, as follows from eq. (2.21). The scale factor ratio \bar{y} is determined by the quartic polynomial (2.25), which in terms of the energy density parameters reads

$$B_3 \bar{y}^4 + (3B_2 - B_4) \bar{y}^3 + 3(B_1 - B_3) \bar{y}^2 + (B_0 - 3B_2 + E^2 \Omega_{\text{m}} + E^2 \Omega_{\text{r}}) \bar{y} - B_1 = 0. \quad (3.6)$$

As last ingredient, we need to determine $\Omega_{\text{de}0}$ as initial condition. In order to do so, we determine the value of the scale factor ratio at present time \bar{y}_0 using the $f_{\mu\nu}$ -Friedmann equation (2.20) evaluated today:

$$0 = B_1 + (3B_2 + \Omega_{\text{k}0} - 1) \bar{y}_0 + 3B_3 \bar{y}_0^2 + B_4 \bar{y}_0^3 \quad (3.7)$$

This polynomial has up to three real-valued roots, out of which we pick the one that satisfies $0 < \bar{y}_0 < \bar{\alpha}$ in order to ensure that we are on the finite branch. Plugging the result into eq. (3.5) evaluated today, determines $\Omega_{\text{de}0}$, which in turn determines $\Omega_{\text{m}0}$ via eq. (3.3).

3.2 Cosmological data

We now present the cosmological observables that are used in our statistical analysis. We use three different types of observations: Supernovae type 1a (SN1a), Baryon Acoustic Oscillations (BAOs) and Cosmic Microwave Background (CMB). Before discussing them in detail, let us first introduce some useful quantities to enlighten the notation.

We start with the definition of the following integral:

$$\mathcal{I}_k(z) = \begin{cases} \frac{1}{\sqrt{|\Omega_{\text{k}0}|}} \sinh \left(\sqrt{|\Omega_{\text{k}0}|} \int_0^z \frac{dz'}{E(z')} \right) & , k < 0 \\ \int_0^z \frac{dz'}{E(z')} & , k = 0, \\ \frac{1}{\sqrt{|\Omega_{\text{k}0}|}} \sin \left(\sqrt{|\Omega_{\text{k}0}|} \int_0^z \frac{dz'}{E(z')} \right) & , k > 0 \end{cases} \quad (3.8)$$

where $E(z) = H(z)/H_0$. We use this quantity to write the various distance indicators, such as the luminosity distance d_{L} and the angular diameter distance d_{A} :

$$d_{\text{L}}(z) = \frac{c}{H_0} (1+z) \mathcal{I}_k(z), \quad d_{\text{A}}(z) = \frac{c}{H_0} \frac{1}{1+z} \mathcal{I}_k(z). \quad (3.9)$$

Another important quantity is the comoving sound horizon, defined as

$$r_{\text{s}}(z) = \frac{c}{\sqrt{3}} \int_z^\infty \frac{dz'}{H(z') \sqrt{1 + (3\Omega_{\text{b}0} / 4\Omega_{\gamma 0}) / (1+z')}}. \quad (3.10)$$

Here $\Omega_{\text{b}0}$ and $\Omega_{\gamma 0}$ are the baryons and photons density parameters. $\Omega_{\gamma 0}$ is fixed by the temperature T_{CMB} of the CMB [129]:

$$\frac{3}{4\Omega_{\gamma 0}h^2} = 31500(T_{\text{CMB}}/2.7\text{K})^{-4}, \quad T_{\text{CMB}} = 2.7255\text{K}. \quad (3.11)$$

Here, $h = H_0/100 \text{ km s}^{-1} \text{ Mpc}^{-1}$ is the normalised Hubble rate today. The photons density parameter is related to the total radiation density parameter via

$$\Omega_{\text{r}0} = \Omega_{\gamma 0}(1 + 0.2271N_{\text{eff}}). \quad (3.12)$$

N_{eff} is the effective number of neutrino species, that we fix to the standard value $N_{\text{eff}} = 3.046$ for our analysis. We now proceed introducing separately the different observables.

3.2.1 Supernovae type 1a

Supernovae of type 1a serve as standard candles whose luminosities can be inferred independently of their redshift. This allows to build up the local distance ladder. We use the catalogue of the Joint Light-curve Analysis (JLA) that contains 740 SN1a events as reported in Ref. [130].

The observed quantity in the case of Supernovae is the apparent magnitude m

$$m = M + 25 + 5 \log_{10} d_{\text{L}} = \mathcal{M} + 5 \log_{10} D_{\text{L}}, \quad (3.13)$$

where M is the absolute magnitude, $D_{\text{L}} = H_0 d_{\text{L}}$ and $\mathcal{M} = M - 5 \log_{10} H_0 + 25$. In this formula \mathcal{M} is just an additive constant and appears as a nuisance parameter. This implies that the absolute magnitude M and H_0 are degenerate parameters.

In order to compare the luminosity distance to the observed apparent magnitude m_{obs} , we have to calibrate the supernovae as [130]

$$m = m_{\text{obs}} - \Delta_{\text{M}} + \alpha X_1 - \beta C, \quad (3.14)$$

where m is related to the luminosity distance as in Eq. (3.13). Here, X_1 and C are the light-curve parameters of the supernova. For the nuisance parameters α , β and Δ_{M} we use the best-fit values $\alpha = 0.140 \pm 0.006$ and $\beta = 3.139 \pm 0.072$ as obtained in Ref. [130]. The parameter Δ_{M} is a correction to the absolute magnitude M of the supernova that depends on the stellar mass M_* of the host galaxy of the supernova as

$$\Delta_{\text{M}} = \begin{cases} -0.060 \pm 0.012 & , \text{ if } M_* < 10^{10} M_{\odot} \\ 0 & , \text{ otherwise.} \end{cases} \quad (3.15)$$

Marginalising over \mathcal{M} , the log-likelihood for the SN-data is given by

$$-2 \log \mathcal{L}_{\text{SN}}(\theta) = S_2 - \frac{S_1^2}{S_0}, \quad (3.16)$$

where we have defined

$$S_0 = \sum_{ij} (C_{\text{SN}}^{-1})_{ij}, \quad S_1 = \sum_{ij} (C_{\text{SN}}^{-1})_{ij} y_i, \quad S_2 = \sum_{ij} (C_{\text{SN}}^{-1})_{ij} y_i y_j, \quad (3.17)$$

in terms of $y = m - 5 \log_{10} D_{\text{L}}$. The covariance matrix C_{SN} is given in Ref. [130]. The errors on α , β and Δ_{M} are added in quadrature.

3.2.2 CMB

CMB observations constrain background cosmology through the measurement of two different distance ratios [131]. The first is the ratio between the angular diameter distance $d_{\text{A}}(z_*)$ and the sound horizon

$r_s(z_*)$ at decoupling epoch z_* . This ratio is measured through the location of the first peak of the CMB power spectrum:

$$l_A = (1 + z_*) \frac{\pi d_A(z_*)}{r_s(z_*)}. \quad (3.18)$$

The second is the angular distance divided by the Hubble horizon at the decoupling epoch, $d_A(z_*)H(z_*)/c$. This last information is usually implemented in the shift parameter, defined as:

$$R(z_*) = H_0 \sqrt{\Omega_{m0}} (1 + z_*) d_A(z_*) / c, \quad (3.19)$$

which differs from $d_A(z_*)H(z_*)/c$ by a factor of $\sqrt{1 + z_*}$. This parameter is obtained assuming

$$H^2(z_*) = H_0^2 \Omega_{m0} (1 + z_*)^3, \quad (3.20)$$

which correspond to neglect all contributions (other than Ω_{m0}) to the evolution history at the time of decoupling $H(z_*)$. We use that the early-universe is not altered in bimetric theory compared to general relativity as our working assumption. This is justified because on the finite branch the energy density arising from the bimetric potential does not contribute to the Hubble rate at large redshifts.

For our statistical analysis we follow the standard procedure [132], implementing CMB data in the three distance priors (l_A , R , $\Omega_{b0}h^2$). We use the latest Planck values [129]

$$l_A(z_*) = 301.471^{+0.089}_{-0.090}, \quad R(z_*) = 1.7502 \pm 0.0046, \quad \Omega_{b0}h^2 = 0.02236 \pm 0.00015 \quad (3.21)$$

In our analysis $R(z_*)$ and $l_A(z_*)$ are computed from eq. (3.19) and eq. (3.18), where the decoupling epoch z_* is obtained via the fitting function [133]:

$$\begin{aligned} z_* &= 1048(1 + 0.00124(\Omega_{b0}h^2)^{-0.738})(1 + g_1(\Omega_{m0}h^2)^{g_2}), \\ g_1 &= \frac{0.0783(\Omega_{b0}h^2)^{-0.238}}{1 + 39.5(\Omega_{b0}h^2)^{0.763}}, \quad g_2 = \frac{0.560}{1 + 21.1(\Omega_{b0}h^2)^{1.81}}. \end{aligned} \quad (3.22)$$

Defining the CMB data vector as

$$X_{\text{CMB}}^T = (l_A - 301.471, R(z_*) - 1.7502, \Omega_{b0}h^2 - 0.02236) \quad (3.23)$$

the likelihood for the CMB is written as:

$$-2 \log \mathcal{L}_{\text{CMB}} = X_{\text{CMB}}^T C_{\text{CMB}}^{-1} X_{\text{CMB}}. \quad (3.24)$$

where the covariance matrix C_{CMB} can be found in [129].

3.2.3 BAO

Barionic Acoustic Oscillations (BAOs) are another important tool to constrain background cosmology. We follow a procedure similar to [107], using measurements at 10 different redshifts $z = 0.106, 0.15, 0.38, 0.51, 0.61, 0.72, 0.978, 1.23, 1.526, 1.944$. The data that we consider are taken from the surveys *6dFGS* [134], *SDSS MGS* [135], *BOSS DR12* [136], *BOSS DR14* [137], *eBOSS QSO* [138] and are summarised, e.g. in table 2 of [107].

The relevant length scale in the case of BAOs is the sound horizon at the drag epoch $r_s(z_d)$. The drag epoch can be derived with the following fitting formula [133]:

$$\begin{aligned} z_d &= \frac{1291(\Omega_{m0}h^2)^{0.251}}{1 + 0.659(\Omega_{m0}h^2)^{0.828}} [1 + b_1(\Omega_{b0}h^2)^{b_2}], \\ b_1 &= 0.313(\Omega_{m0}h^2)^{-0.419} [1 + 0.607(\Omega_{m0}h^2)^{0.674}], \quad b_2 = 0.238(\Omega_{m0}h^2)^{0.223} \end{aligned} \quad (3.25)$$

The other relevant quantities in our study are the effective distance measure d_V and the redshift-weighted comoving distance d_M :

$$d_V(z) = \left[(1 + z)^2 d_A^2(z) \frac{cz}{H(z)} \right]^{1/3}, \quad d_M(z) = (1 + z) d_A(z). \quad (3.26)$$

The likelihood for the statistical analysis is derived using the covariance matrices taken from the original references [134–138].

3.3 Statistical analysis and results

Using the aforementioned data sets, we perform a statistical analysis via MCMC sampling for all models with up to three non-vanishing interaction and vacuum energy parameters β_n . The Λ CDM-model corresponds to the β_0 -model in this sense. We classify models according to their number of free parameters β_n : models with one, two or three free parameters β_n are referred to as one-, two- or three-parameter models, respectively. In terms of the physical parameters, that means that one, two or all three of the parameters $\bar{\alpha}$, Ω_{FP} and Ω_Λ are independent. The best-fit values and the 1-dimensional (1σ) error intervals for all free and derived parameters are reported in tables 1 and 2.

In order to estimate the goodness-of-fit for each model, we compute the Bayesian Information Criterion (BIC) [139],

$$\text{BIC} = \chi^2 + k \ln N \quad (3.27)$$

where $\chi^2 = -2 \ln \mathcal{L}$ is evaluated at maximum likelihood, k is the number of model parameters and N is the number of data points. For our combined data set SN+CMB+BAO we have $N = 740 + 3 + 10 = 753$. The number of model parameters is given by $k = 3 + \hat{k}$ with \hat{k} the number of independent physical parameters as will become clear from the next paragraph. We will use the BIC of the Λ CDM-model as reference. The difference ΔBIC allows to estimate the preference of one model over another as [107, 140]: strong support ($\Delta\text{BIC} < -12$), favorable ($\Delta\text{BIC} < -6$), inconclusive ($\Delta\text{BIC} < 6$), disfavored ($\Delta\text{BIC} < 12$), strongly disfavored ($\Delta\text{BIC} \geq 12$). The corresponding ΔBIC are reported in tables 1 and 2 as well.

Independent parameters and priors. We use the theoretical bounds of [105] that ensure a consistent cosmology, which we summarise in table 4, as flat priors. For the parameter Ω_Λ we use $[0, 1]$ as flat prior. For the other physical parameters $\bar{\alpha}$ and Ω_{FP} we use a log-scale to resolve large regions of the parameter space. We again use flat priors with $\log_{10}(\bar{\alpha}) \in [-100, 100]$ and $\log_{10}(\Omega_{\text{FP}}) \in [-2, 122]$ if applicable¹⁰. The lower bound on Ω_{FP} is chosen because of the Higuchi bound, while the upper bound corresponds to the Planck-scale. In addition to the physical parameters, the models further depend on the cosmological parameters. We choose to scan over H_0 , Ω_{k0} and Ω_{b0} as free parameters with flat priors $[45 \frac{\text{km/s}}{\text{Mpc}}, 85 \frac{\text{km/s}}{\text{Mpc}}]$, $[0, 1]$ and $[0, 1]$, respectively. Note that we analytically marginalise over H_0 in the case of supernovae. The other energy density parameters $\Omega_{\text{de}0}$ and $\Omega_{\text{m}0}$ are computed from eqs. (3.3) and (3.5). We use $[-1, 1]$ and $[0, 1]$ as flat priors on these parameters, respectively.

Reference model and consistency of data sets. Let us start with a discussion of the results for the Λ CDM-model as reference. The 1- and 2-dimensional posterior distributions for the parameters H_0 , $\Omega_{\text{m}0}$ and $\Omega_\Lambda = \Omega_{\text{de}0}$ are presented in the left panel of fig. 1. While supernovae do not constrain H_0 due to the degeneracy with the absolute magnitude, also CMB and BAOs do not yield robust constraints individually. However, this geometric degeneracy is broken when combining all three sets of data. We then obtain the value $H_0 = (68.8 \pm 1.2)\text{km/s/Mpc}$, which is in good agreement with current constraints [5, 130, 141]. Our value is slightly but not significantly larger, which can be understood as an artifact of using the distance priors [129]. Combining the data sets stabilises spatial curvature to the value $\Omega_{k0} = 0.002 \pm 0.003$ such that the universe is spatially flat within 68% c.l. Also the other parameters as reported in table 1 are in good agreement with current constraints. We conclude that our analysis is robust. At the best-fit point we have $\chi^2 = 694.7$ leading to $\text{BIC} = 721.2$.

3.3.1 β_1 -model

As discussed before, the β_1 -model is the only bimetric one-parameter model that can possibly give rise to a viable expansion history. The posterior distributions are presented in the right panel of fig. 1. Also this model is subject to the geometric degeneracy such that both H_0 and Ω_{k0} are unconstrained by CMB and BAO individually. Combining all three data sets stabilises these parameters. Data then favors a slightly spatially curved universe with $\Omega_{k0} = -0.007^{+0.004}_{-0.003}$. The Hubble rate today is constrained to the remarkable high value of $H_0 = 73.1^{+1.6}_{-1.4}\text{km/s/Mpc}$, which is in perfect agreement with local determinations of H_0 [142]. We emphasise that we obtained this result without local prior

¹⁰The Λ CDM-model does not contain these parameters. For the two-parameter models, $\bar{\alpha}$ and Ω_{FP} are not independent. For the $\beta_0\beta_1$ -model we scan over the parameter $\log_{10}(\bar{\alpha})$, while we scan over $\log_{10}(\Omega_{\text{FP}})$ for the $\beta_1\beta_{2,3,4}$ -models.

Model	β_0	β_1	$\beta_0\beta_1$	$\beta_1\beta_n$
$\bar{\alpha}$		$3^{-1/2}$	< 0.2	< 0.016
m_{FP} [eV]		$(1.82 \pm 0.02) \times 10^{-32}$	$(1.33 \pm 0.02) \times 10^{-32}$	$> 4.24 \times 10^{-31}$
Λ [10^{-64}eV^2]	1.76 ± 0.05	2.5 ± 0.1	1.8 ± 0.1	$1.76^{+0.1}_{-0.09}$
H_0 [$\frac{\text{km/s}}{\text{Mpc}}$]	$68.8^{+1.4}_{-1.2}$	$73.1^{+1.6}_{-1.4}$	68.8 ± 0.2	69.0 ± 1.0
Ω_Λ	0.69 ± 0.01	0.86 ± 0.01	$0.69^{+0.03}_{-0.02}$	0.69 ± 0.01
$\Omega_{\text{m}0}$	0.31 ± 0.01	0.27 ± 0.01	0.31 ± 0.02	0.31 ± 0.01
$\Omega_{\text{de}0}$	0.69 ± 0.01	0.73 ± 0.01	0.69 ± 0.02	0.69 ± 0.01
$\Omega_{\text{k}0}$	$0.002^{+0.004}_{-0.003}$	$-0.007^{+0.004}_{-0.003}$	$0.002^{+0.005}_{-0.001}$	0.002 ± 0.004
$\Omega_{\text{b}0}$	0.0224 ± 0.0001	0.0223 ± 0.0003	0.0224 ± 0.0004	0.0224 ± 0.0003
χ^2	694.7	726.0	694.7	694.7
ΔBIC	721	+31	+6.6	+6.6

Table 1. The best-fit values and errors at 68% c.l. from SN+CMB+BAO for the one- and two-parameter models are shown. To compute the values of m_{FP} and Λ from Ω_{FP} and Ω_Λ , we use the obtained value of H_0 for each model. The β_0 -model is the Λ CDM-model and hence does not contain the parameters $\bar{\alpha}$ and m_{FP} . The last row contains the parameter values for the $\beta_1\beta_2$ -, $\beta_1\beta_3$ - and $\beta_1\beta_4$ -model as indicated by the subscript n , for which the statistical analysis yielded the exact same results as expected.

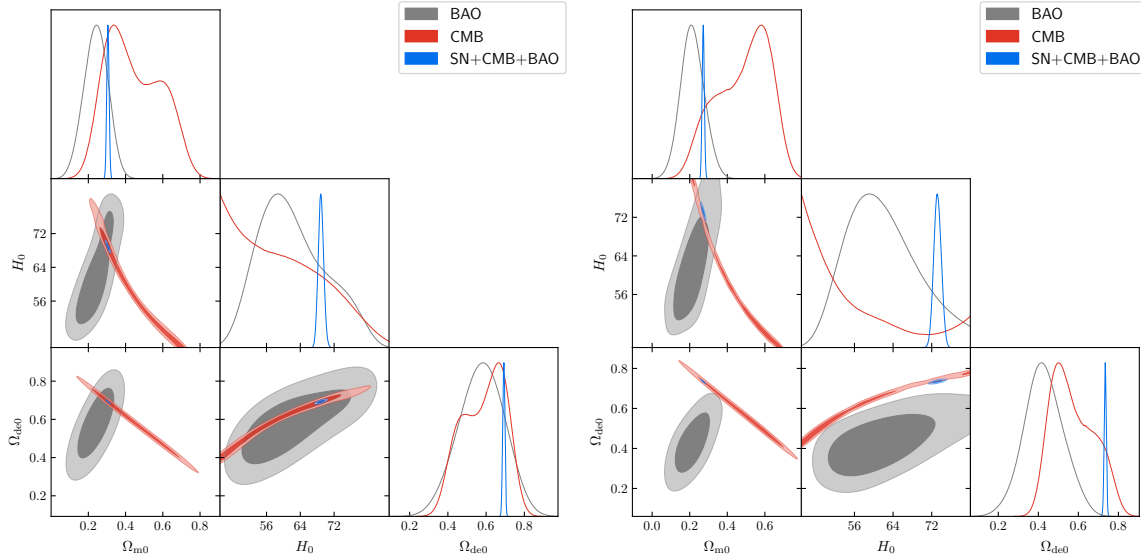


Figure 1. Marginalised posterior distribution of the cosmological parameters in the Λ CDM-model (left) and the β_1 -model (right). The contour lines correspond to 68% and 95% c.l. The results reflect a tension between the early- and late-time data sets for the β_1 -model.

on H_0 . The value of the spin-2 mass is constrained to be small with $m_{\text{FP}} = (1.82 \pm 0.02) \times 10^{-32}$ eV, which is close to the Higuchi bound.

However, the cosmological early- and late-time measurements are incompatible within this model, as can be seen already from the right panel of fig. 1. Quantitatively, $\Delta\text{BIC} = +31$ indicates that this model is indeed strongly disfavored by cosmological background data. Therefore, this model does not solve the H_0 -tension, despite its large favored value. We conclude that the bimetric β_1 -model is statistically ruled out. Nonetheless, we summarise the obtained best-fit values for the other parameters in table 1.

Model	$\beta_0\beta_1\beta_4$	$\beta_0\beta_1\beta_3$	$\beta_0\beta_1\beta_2$
$\bar{\alpha}$	< 0.14	< 0.03	< 0.06
m_{FP} [eV]	$> 1.01 \times 10^{-32}$	$> 1.17 \times 10^{-32}$	$> 1.08 \times 10^{-32}$
Λ [10^{-64}eV^2]	$1.77^{+0.10}_{-0.09}$	1.77 ± 0.09	$1.77^{+0.10}_{-0.09}$
H_0 [$\frac{\text{km/s}}{\text{Mpc}}$]	$68.8^{+1.5}_{-1.3}$	$68.9^{+1.4}_{-1.3}$	$68.9^{+1.4}_{-1.3}$
Ω_Λ	$0.69^{+0.02}_{-0.01}$	$0.69^{+0.02}_{-0.01}$	$0.69^{+0.03}_{-0.01}$
$\Omega_{\text{m}0}$	0.31 ± 0.01	0.30 ± 0.01	0.31 ± 0.01
$\Omega_{\text{de}0}$	0.69 ± 0.01	0.69 ± 0.01	0.69 ± 0.01
$\Omega_{\text{k}0}$	0.002 ± 0.004	$0.002^{+0.004}_{-0.003}$	$0.002^{+0.006}_{-0.001}$
$\Omega_{\text{b}0}$	0.0224 ± 0.0003	0.0224 ± 0.0003	0.0224 ± 0.0003
χ^2	694.7	694.7	694.7
ΔBIC	+11.6	+11.6	+11.6

Model	$\beta_1\beta_2\beta_3$	$\beta_1\beta_2\beta_4$	$\beta_1\beta_3\beta_4$
$\bar{\alpha}$	< 0.004	< 0.01	< 0.002
m_{FP} [eV]	$> 1.10 \times 10^{-32}$	$> 1.15 \times 10^{-32}$	$> 1.10 \times 10^{-32}$
Λ [10^{-64}eV^2]	$1.78^{+0.09}_{-0.1}$	1.77 ± 0.09	$1.77^{+0.10}_{-0.09}$
H_0 [$\frac{\text{km/s}}{\text{Mpc}}$]	$68.9^{+1.4}_{-1.3}$	$69.0^{+1.3}_{-1.2}$	$68.9^{+1.4}_{-1.3}$
Ω_Λ	0.69 ± 0.01	0.69 ± 0.01	0.69 ± 0.01
$\Omega_{\text{m}0}$	0.31 ± 0.01	0.30 ± 0.01	0.31 ± 0.01
$\Omega_{\text{de}0}$	0.69 ± 0.01	0.69 ± 0.01	0.69 ± 0.01
$\Omega_{\text{k}0}$	0.002 ± 0.004	$0.0023^{+0.0003}_{-0.004}$	0.002 ± 0.003
$\Omega_{\text{b}0}$	0.0224 ± 0.0003	0.0224 ± 0.0003	0.0224 ± 0.0003
χ^2	694.7	694.7	694.7
ΔBIC	+11.6	+11.6	+11.6

Table 2. The best-fit values and errors at 68% c.l. from SN+CMB+BAO for the three-parameter models are shown. To compute the values of m_{FP} and Λ from Ω_{FP} and Ω_Λ , we use the obtained value of H_0 for each model.

3.3.2 Two-parameter models

As already discussed, consistency of the early universe on the finite branch requires $\beta_1 > 0$. This means that there are four possibilities for the two-parameter models: the $\beta_0\beta_1$ model and the $\beta_1\beta_n$ models with $n = 2, 3, 4$. From our analysis it emerges that the results for all the $\beta_1\beta_n$ models are very similar and statistically compatible. For this reason, we explicitly show only the results for the $\beta_1\beta_3$ model and we refer to it as $\beta_1\beta_n$ for the rest of this section. In fig. 2 we plot the 1- and 2-dimensional marginalised posterior distribution for these models, where we can see that the data sets are compatible. This is true also for SN data, that are not shown explicitly in this figure. We conclude that the data sets can be combined in the statistical analysis.

In table 1 we summarise the results of the combined analysis. The main difference between the $\beta_0\beta_1$ model and the $\beta_0\beta_n$ models are the values of $\bar{\alpha}$ and m_{FP} . In both cases, $\bar{\alpha}$ is constrained only from above with a maximum value of 0.2 for the $\beta_0\beta_1$ model and 0.016 for the $\beta_1\beta_n$ models. In the $\beta_0\beta_1$ model the value of m_{FP} is constrained to be $(1.33 \pm 0.02) \times 10^{-32}$ eV, which lies close to the Higuchi bound. In the $\beta_1\beta_n$ models, however, the value of the Fierz-Pauli mass is constrained only weakly from below with $m_{\text{FP}} > 4.24 \times 10^{-31}$ eV. We will discuss the constraints on $\bar{\alpha}$ and m_{FP} in

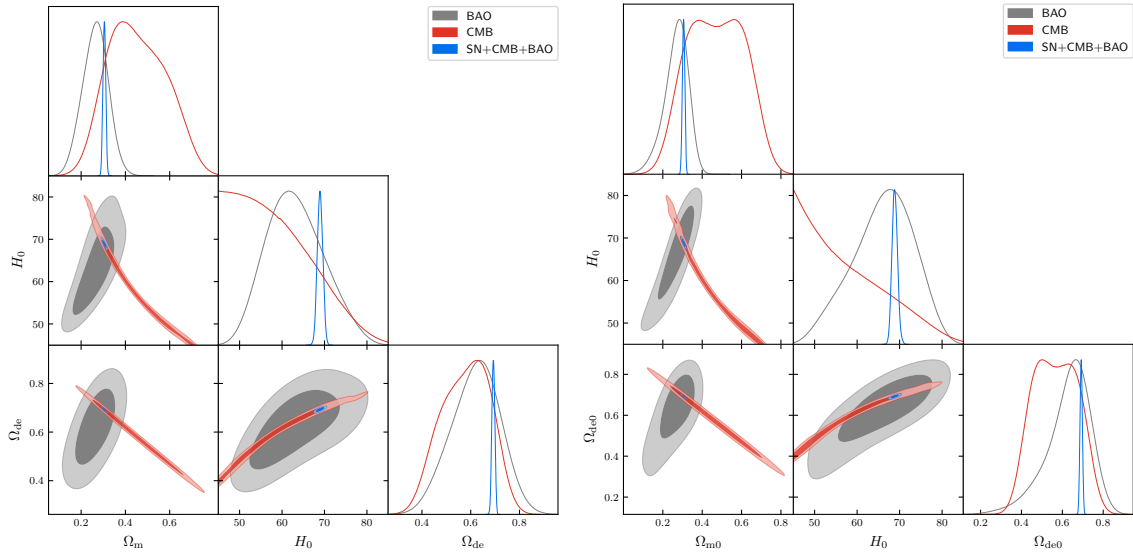


Figure 2. Marginalised posterior distribution of the cosmological parameters in the $\beta_0\beta_1$ -model (left) and the $\beta_1\beta_3$ -model (right). The contour lines correspond to 68% and 95% c.l.

more detail in section 4.3, where we will compare the results of the statistical analysis with local tests of gravity.

Despite these differences, the other parameters for the $\beta_0\beta_1$ and $\beta_1\beta_n$ models are very similar with each other and compatible with Λ CDM. The only exception is spatial curvature, that seems to be slightly positive for the $\beta_0\beta_1$ model. However, this model still prefers an almost flat universe with $\Omega_{k0} = 0.002^{+0.005}_{-0.001}$, which remains very close to 0 at 1σ and compatible with the Λ CDM value. Moreover, the value of χ^2 in both models coincides with Λ CDM. This makes the $\beta_0\beta_1$ and $\beta_1\beta_n$ models slightly disfavored with a $\Delta\text{BIC} = +6.6$, since these models have more free parameters with respect to Λ CDM.

3.3.3 Three-parameter models

We finish by discussing models with three free parameters. We will see that the parameter constraints are similar across these models. Data sets are compatible for all the three parameter models, as we can see in figs. 3 to 5. Therefore, combining the data sets for these models is trustworthy¹¹.

- *Models with $\beta_4 = 0$.* We first discuss the three-parameter models without vacuum energy in the f -sector. We present the 1- and 2- dimensional marginalised posterior distribution in the left and right panel of fig. 3 and the left panel of fig. 4 for the $\beta_0\beta_1\beta_2$ -, $\beta_0\beta_1\beta_3$ - and $\beta_0\beta_1\beta_4$ -model, respectively. The parameter constraints are reported in table 2 and agree with the Λ CDM values within 1σ and are all quite similar across these models. The only exception is that the $\beta_0\beta_1\beta_2$ -model seems to prefer a slightly curved universe at 1σ . However, the value of the curvature is very small and compatible with Λ CDM at 1σ and therefore we do not consider it as a statistically relevant difference. The bimetric parameters $\bar{\alpha}$ and m_{FP} are constrained only weakly. We will discuss more about the constraints on these parameters in the $\bar{\alpha} - m_{\text{FP}}$ plane when comparing with local tests in section 4.3. We find that these models are consistent with the current data because $\chi^2 = 694.7$ as in the Λ CDM-model. However, the BIC is higher due to the two additional free parameters indicating that these models are statistically disfavored.

- *Models with $\beta_0 = 0$.* The result for this models is very similar to models with $\beta_4 = 0$. The only exception is that $\bar{\alpha}$ is more constrained of about one order of magnitude, as it can be seen in table 2. We show the 1- and 2- dimensional marginalised posterior distribution in the right panel of fig. 4 for

¹¹This is true also for SN data, even if they are not shown explicitly in figs. 3 to 5.

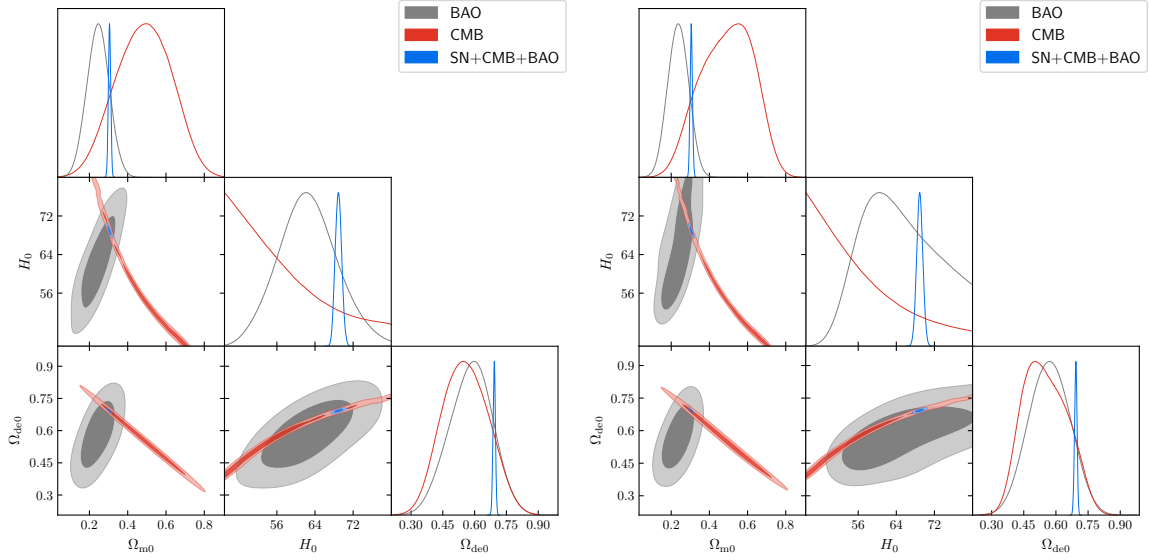


Figure 3. Marginalised posterior distribution of the cosmological parameters in the $\beta_0\beta_1\beta_2$ -model (left) and the $\beta_0\beta_1\beta_3$ -model (right). The contour lines correspond to 99% and 95% c.l.

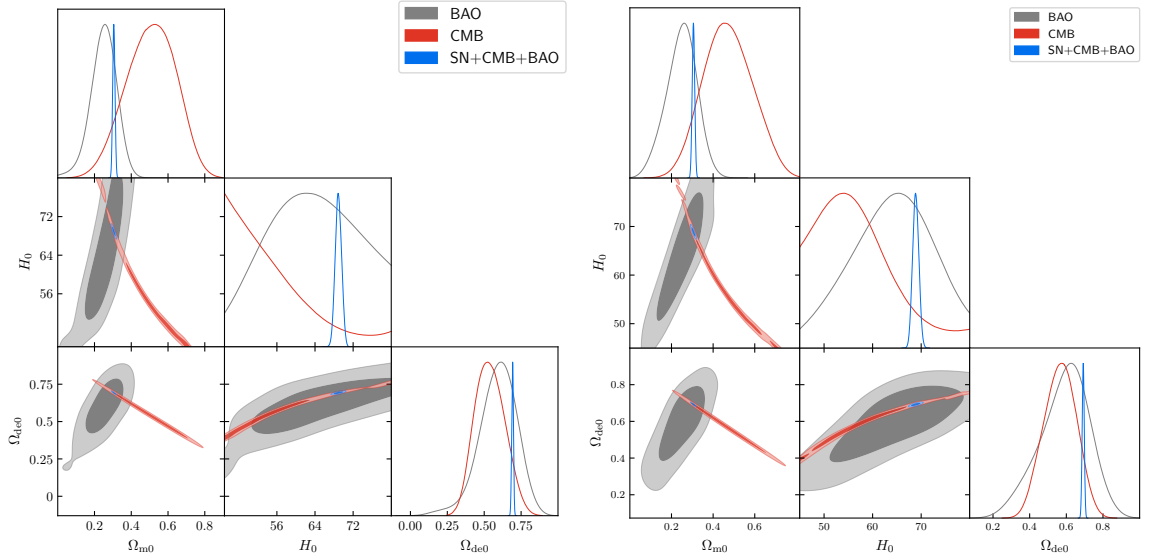


Figure 4. Marginalised posterior distribution of the cosmological parameters in the $\beta_0\beta_1\beta_4$ -model (left) and the $\beta_1\beta_2\beta_3$ -model (right)

the $\beta_1\beta_3\beta_4$ -model and in fig. 5 for the $\beta_1\beta_2\beta_4$ - and $\beta_1\beta_3\beta_4$ -model. Again, these models have the same χ^2 of the Λ CDM-model, which makes them statistically disfavored with a higher BIC.

4 Bounds from local tests of gravity

Having identified those regions of the parameter space that are in agreement with current observations in background cosmology, we now turn to local tests of gravity. In section 4.1 we give a brief review on local tests of gravity and present the existing constraints on the parameters \bar{a} and m_{FP} . However, the existing bounds were derived without taking into account the Vainshtein screening mechanism.

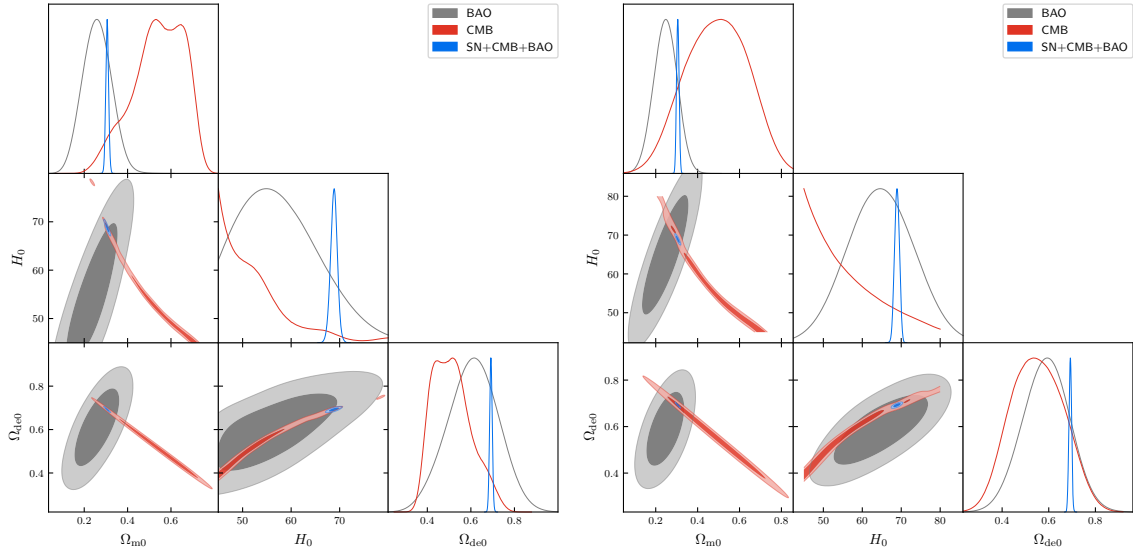


Figure 5. Marginalised posterior distribution of the cosmological parameters in the $\beta_1\beta_2\beta_4$ -model (left) and the $\beta_1\beta_3\beta_4$ -model (right)

In regions where Vainshtein screening is active, the bounds on $\bar{\alpha}$ and m_{FP} are not trustworthy. In section 4.2 we identify the regions of the parameter space that give rise to Vainshtein screening in spherically symmetric systems. We finally confront cosmological with local bounds in section 4.3 in parameter regions without Vainshtein screening.

4.1 Local tests of gravity

In this section we briefly summarise local tests of gravity. For details and reviews we refer to Ref. [108–111, 113]. Extra degrees of freedom (such as the massive spin-2 field of bimetric theory) modify the Newtonian gravitational potential as compared to GR. This is usually attributed to a *fifth force*. If the force mediator is massive, it contributes a Yukawa potential to the gravitational potential felt by a massive test body. Following standard notation in the literature, the gravitational potential for a static and spherically-symmetric configuration around a massive source can be parametrised as

$$V(r) = -\frac{1}{m_{\text{P}}} \left(\frac{1}{r} + \xi \frac{e^{-r/\lambda}}{r} \right), \quad (4.1)$$

with m_{P} the Planck mass. This is referred to as Yukawa parametrisation. The first term corresponds to the usual potential arising from massless gravitons. The second term arises from a massive force mediator with Compton wavelength λ and coupling to matter ξ . While in the limit $\xi \ll 1$ the fifth force is suppressed, it is most prominent on length scales $r \sim \lambda$. As we will see in section 4.2, these parameters are related to the bimetric parameters as

$$\xi = \frac{4\bar{\alpha}^2}{3}, \quad \lambda = m_{\text{FP}}^{-1}. \quad (4.2)$$

In fig. 6 we present the constraints from local tests of gravity on the bimetric parameters $\bar{\alpha}$ and m_{FP} as indicated by the black lines. The gray-shaded region is excluded by 95% c.l. To compute the constraints, we follow the procedure as described in [108–110]. The laboratory constraints correspond to the Irvine [143]¹², Eöt-Wash [145] and Stanford [146] experiments. The geophysical constraints correspond to the lake [147, 148] and tower [149–151] experiments. The constraints from measurements

¹²Note that the bound from [144] is not included, yet.

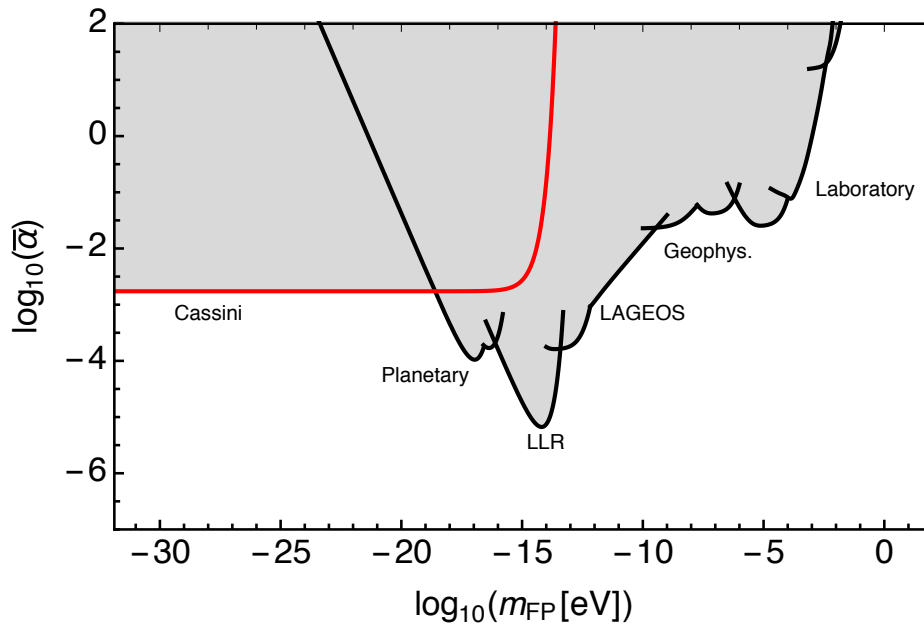


Figure 6. Bounds on the bimetric parameters $\bar{\alpha}$ and m_{FP} from local tests of gravity. The black lines result from tests of the Newtonian gravitational potential as reported in [108–110, 145, 146, 155]. Tests of the scalar curvature yield the red line [91, 112]. The gray-shaded region is excluded by 95% c.l. Note that the Vainshtein mechanism is not taken into account in the derivation of these bounds.

with the LAGEOS satellite are reported in [152–154]. The constraint from Lunar-Laser-Ranging (LLR) results from lunar precession [109]. The planetary constraints are reported in [155].

The aforementioned tests of the Newtonian potential provide only weak constraints on modifications if the mass of the fifth force mediator is small. In this region of the parameter space, tests of the scalar curvature, i.e. the deflection and delay of light induced by matter, provide powerful constraints. We use the gravitational slip parameter γ , which is unity in GR, $\gamma = 1$. Within the context of bimetric theory, the parameter has been calculated to be [91]

$$\gamma = \frac{3 + 2\bar{\alpha}^2 e^{-m_{\text{FP}} r}}{3 + 4\bar{\alpha}^2 e^{-m_{\text{FP}} r}}. \quad (4.3)$$

The most precise value has been obtained within the solar system. The measurement of the time delay of radar signals sent between the Earth and the Cassini spacecraft on its way to Saturn yields $\gamma - 1 = (2.1 \pm 2.3) \times 10^{-5}$ [112]. The radio signals were passing by the sun at a distance of 1.6 solar radii, i.e. $r \simeq 7.44 \times 10^{-3} \text{ AU} \simeq 1.31 \times 10^{-15} \text{ eV}^{-1}$. Using these values defines the red line in fig. 6. The region above that line is excluded by 95% c.l. For small spin-2 masses, the coupling to matter is constrained to be $\bar{\alpha} \lesssim 1.7 \times 10^{-3}$. A collection of bounds on γ from time delay and deflection of light from galaxy halo to solar system scales can be found in [113], which however are less constraining than the bound used here.

Summarising, the most stringent constraint comes from LLR with $\bar{\alpha} < 8.9 \times 10^{-6}$ at 95% c.l. for $m_{\text{FP}} \simeq 6.5 \times 10^{-15} \text{ eV}$. On the other hand, for $m_{\text{FP}} \gtrsim 10^{-2} \text{ eV}$ the bounds on $\bar{\alpha}$ are weak. This, however, is not the end of the story in the framework of bimetric theory due to the Vainshtein screening mechanism as we discuss in the next section.

4.2 Vainshtein screening

Local tests of gravity put tight constraints on modifications of the gravitational potential. Historically, the linear theory of Fierz and Pauli [39] was discarded because it did not pass basic solar system tests. This is due to the so-called vDVZ discontinuity [40, 41]: the helicity-0 mode of the massive graviton

couples to the trace of the energy-momentum tensor even in the limit $m_{\text{FP}} \rightarrow 0$. Vainshtein argued that including nonlinear interaction terms for the massive spin-2 field restores GR in that limit thus curing the problem [42]. This is indeed the case as explicitly demonstrated in [156–158]. For a review on the Vainshtein mechanism we refer to [159].

Bimetric theory incorporates the Vainshtein mechanism as explicitly demonstrated for static and spherically symmetric systems [89, 90, 93, 160]. We leave the technical details to appendix B, where we repeat and extend the analysis by relaxing the assumption of asymptotic flatness to allow for a non-vanishing cosmological constant. Here we limit ourselves to discussing the general features. The radius below which nonlinearities have to be taken into account is referred to as Vainshtein radius $r_V = (r_S/m_{\text{FP}}^2)^{1/3}$ with r_S the Schwarzschild radius of the matter source. For larger radii, $r \gg r_V$, the linear approximation is valid. The resulting gravitational potential for small and large radii can be written as [89, 93]

$$V(r) = \begin{cases} -\frac{1}{m_g^2} \frac{1}{r} & r \ll r_V \\ -\frac{1}{m_P^2} \left(\frac{1}{r} + \frac{4\bar{\alpha}^2}{3} \frac{e^{-m_{\text{FP}} r}}{r} \right) & r \gg r_V \end{cases}, \quad (4.4)$$

where $m_P^2 = (1 + \bar{\alpha}^2)m_g^2$ is the unscreened Planck mass. This justifies our identification (4.2). On the other hand, since r_V depends on the spin-2 mass and the mass of the central source, the constraints on $\bar{\alpha}$ and m_{FP} summarised in fig. 6 are not trustworthy.

However, Vainshtein screening exists only in a subregion of the parameter space [90, 93], as we review in appendix B. In this section, we will identify this subregion in terms of $\bar{\alpha}$ and m_{FP} . The Vainshtein mechanism relies on the following three necessary conditions:

- *Consistent screening regime.* The existence of a nonlinear solution that restores GR in spacetime regions close to the matter source requires

$$\frac{c^3 \beta_3}{c\beta_1 + 2c^2\beta_2 + c^3\beta_3} > 1. \quad (4.5)$$

Since the denominator is positive if $m_{\text{FP}}^2 > 0$, this bound implies that β_3 must be strictly positive¹³, $\beta_3 > 0$. That means, any bimetric model with $\beta_3 = 0$ does not have a working Vainshtein mechanism (for some related caveats, see [93]).

- *Consistent asymptotics.* The nonlinear equations must give rise to a solution that matches the linearised solution for $r \gg r_V$. This requires

$$\frac{c^2\beta_2 + c^3\beta_3}{c\beta_1 + 2c^2\beta_2 + c^3\beta_3} < \sqrt{\frac{c^3\beta_3}{c\beta_1 + 2c^2\beta_2 + c^3\beta_3}} \quad (4.6)$$

to be satisfied. Combined with eq. (4.5) it follows that β_2 must be strictly negative, $\beta_2 < 0$. Bimetric models with $\beta_2 = 0$ do not give rise to Vainshtein screening.

- *Consistent Vainshtein-Yukawa solution.* The nonlinear solution realising Vainshtein screening has to be smoothly connected to the linear solution realising the Yukawa-type fifth force without branch cuts. The existence of such a well-defined Vainshtein-Yukawa solution imposes another restriction on the parameters. The explicit expression is lengthy so that we shift its presentation to eq. (B.28).

Following [105], we express these conditions in terms of the physical parameters $\bar{\alpha}$, m_{FP} , and Λ in this section. The relations between the interaction and physical parameters are collected in appendix A. It suffices to study models with all interaction parameters β_1 , β_2 and β_3 being free as only those models can possibly give rise to a viable cosmic expansion history while incorporating the local Vainshtein mechanism.

¹³Recall that the infinite branch solution in the context of background cosmology is well-defined only for $\beta_3 < 0$. Hence, requiring of a working Vainshtein mechanism rules out the infinite branch.

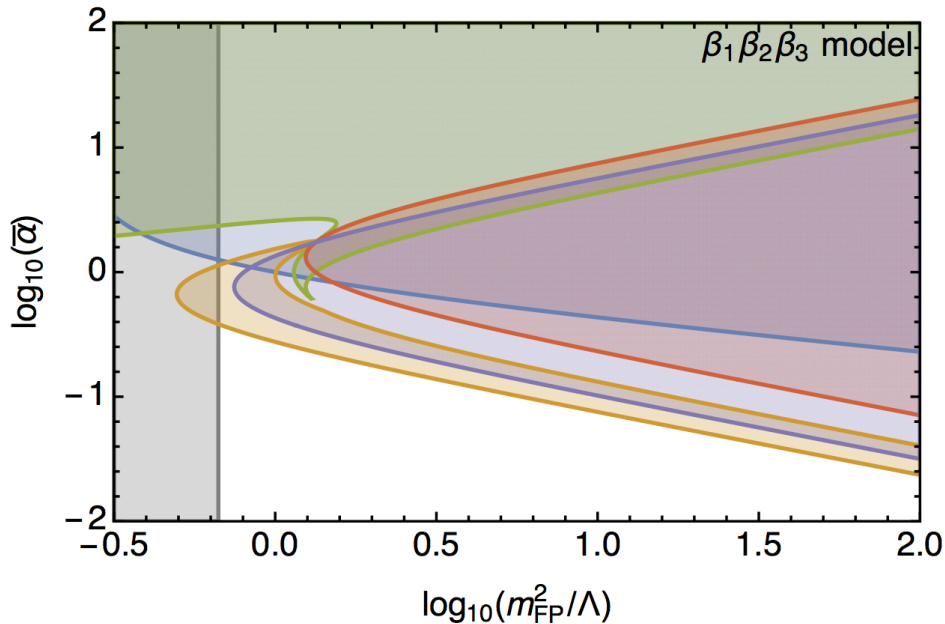


Figure 7. The physical parameter space of the $\beta_1\beta_2\beta_3$ model is shown. The model gives rise to a consistent cosmology only outside the blue-shaded region, which indicates where the vacuum point is not well-defined, and the red-shaded region, in which β_1 is non-positive. The Vainshtein mechanism works only outside the purple-shaded region, which does not give rise to a consistent screening regime, the green-shaded region, which indicates where the Vainshtein solution does not have the right asymptotics, and the yellow-shaded region, in which there is no Vainshtein-Yukawa solution. Finally, the Higuchi bound is violated in the gray-shaded region. Summarising, this bimetric model gives rise to a viable expansion history while incorporating a working Vainshtein mechanism in the region that is left white.

Cosmologically viable one- and two-parameter models are not able to incorporate Vainshtein screening. The $\beta_1\beta_2\beta_3$ -model is the only three-parameter model with a possibly viable background cosmology and a working Vainshtein mechanism. In fig. 7 we collect all the aforementioned theoretical bounds on the physical parameter space of that model. The expressions are too lengthy to display them here explicitly. The blue- and red-shaded regions are excluded as these do not give rise to a viable expansion history. The purple-shaded region violates the bound in eq. (4.5). In the green-shaded region the bound in eq. (4.6) is violated. The Vainshtein-Yukawa solution does not exist in the yellow-shaded region, which represents the most stringent bound. To summarise, we expand the most-stringent bound on the physical parameters for $m_{\text{FP}}^2 \gg \Lambda$ to find

$$16\bar{\alpha}^2 m_{\text{FP}}^2 \lesssim \Lambda. \quad (4.7)$$

If this approximate bound is satisfied, the $\beta_1\beta_2\beta_3$ -model incorporates the local Vainshtein mechanism. As can be seen from fig. 7, the parameter region giving rise to a viable cosmic expansion history is only slightly larger.

Before moving on, let us point out the following caveats. The equivalence principle is violated in two-body systems due to nonlinearities [161]. The assumption of spherical symmetry entering the derivation of the gravitational potential might not be appropriate to describe, e.g. the earth-moon system. Further, Vainshtein screening is weaker or even completely absent in systems with cylindrical or planar symmetry, respectively, as demonstrated in the context of galileons [162]. This has to be taken into account for gravity tests without spherical symmetry.

4.3 Local vs. cosmological bounds

We are finally in the position to compare the constraints from local tests of gravity, shown in fig. 6, to the parameter regions that give rise to Vainshtein screening. Further, we compare the local constraints

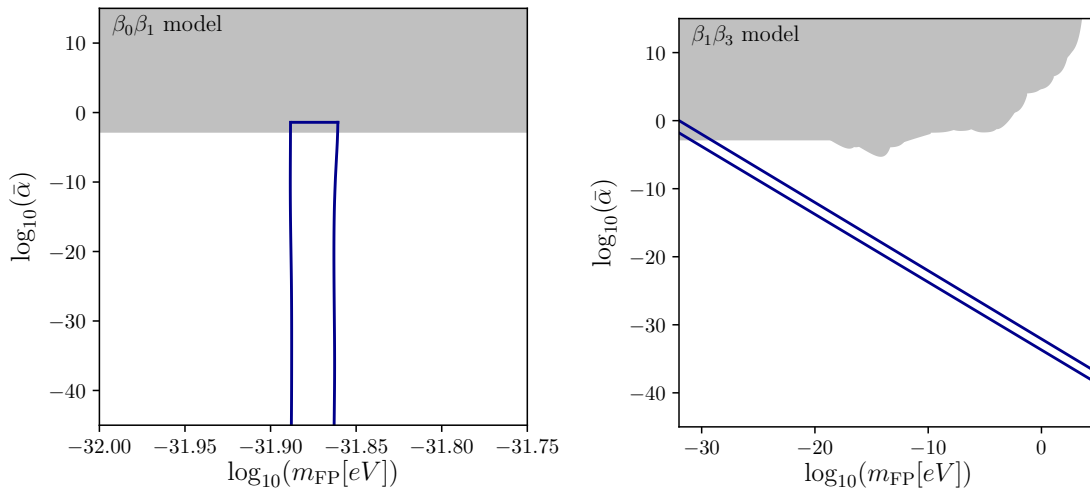


Figure 8. Cosmological constraints compared to local tests for the $\beta_0\beta_1$ -model (left) and for the $\beta_1\beta_3$ -model (right). The blue lines delimit the 2σ regions from the statistical analysis. The gray region is excluded by local tests at 2σ .

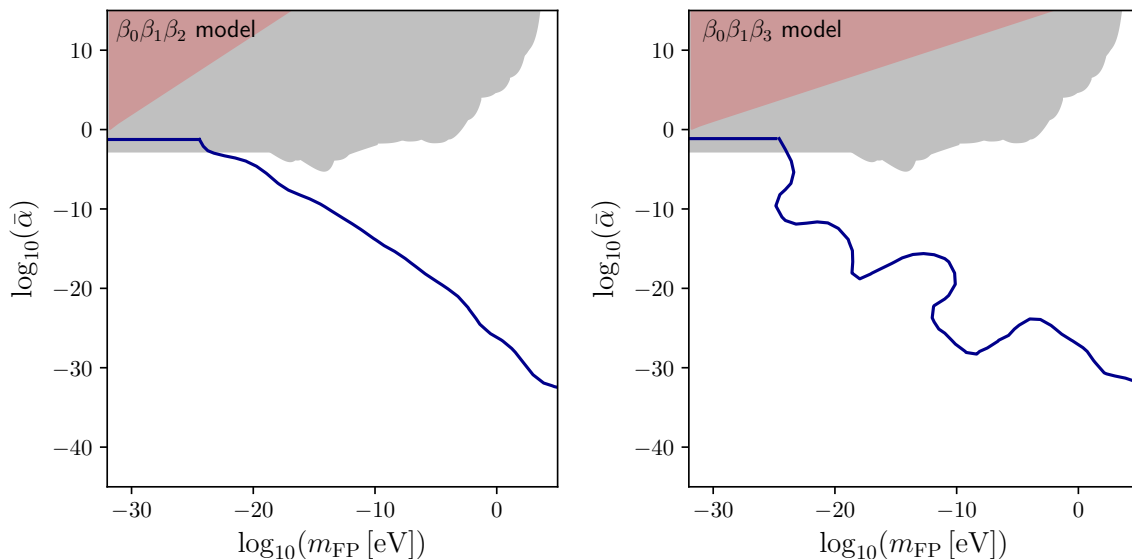


Figure 9. The combined bounds from local and cosmological tests for the $\beta_0\beta_1\beta_2$ - (left) and $\beta_0\beta_1\beta_3$ -model (right). The gray-shaded region is excluded by local tests of gravity at 95% c.l. The red-shaded region is excluded by theoretical constraints. The region above the blue line is excluded by our bounds from cosmology at 95% c.l.

to the constraints that we inferred from background cosmology in section 3.3. Since only the $\beta_1\beta_2\beta_3$ -model incorporates Vainshtein screening, the local bounds are directly applicable to all the other models considered in this paper. The discussed observational bounds in this section always refer to 95% confidence level.

Let us start discussing the β_1 -model. As mentioned before, the cosmological data sets are not compatible, strongly disfavoring this model. If we nonetheless combine the data sets, the spin-2 mass is constrained to $m_{\text{FP}} = (1.82 \pm 0.02) \times 10^{-32}$ eV. The coupling to matter is fixed to the value

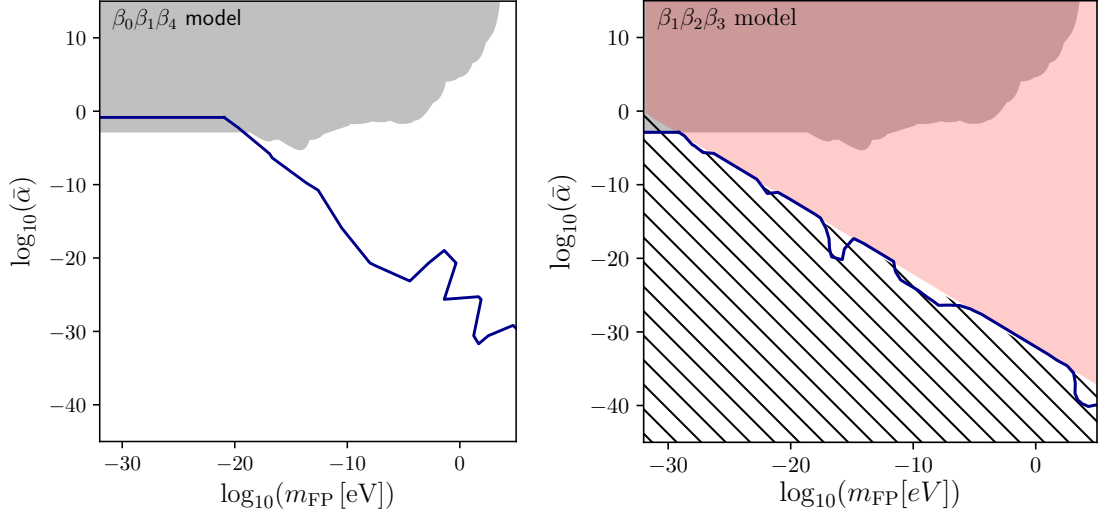


Figure 10. The combined bounds from local and cosmological tests for the $\beta_0\beta_1\beta_4$ - and $\beta_1\beta_2\beta_3$ -model. The gray-shaded region is excluded by local tests of gravity at 95% c.l. The red-shaded region is excluded by theoretical constraints. The region above the blue line is excluded by our bounds from cosmology at 95% c.l. The hatched region in the right panel represents where the Vainshtein mechanism is working.

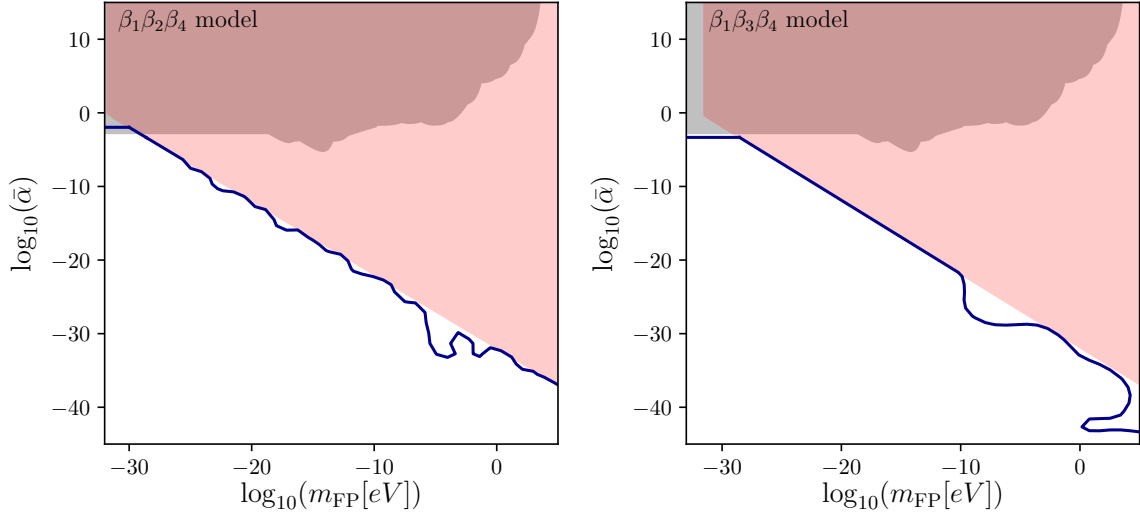


Figure 11. The combined bounds from local and cosmological tests for the $\beta_1\beta_2\beta_4$ - and $\beta_1\beta_3\beta_4$ -model. The region above the gray line is excluded by local tests of gravity at 95% c.l. The red-shaded region is excluded by theoretical constraints. The region above the blue line is excluded by our bounds from cosmology at 95% c.l.

$\bar{\alpha} = 1/\sqrt{3} \simeq 0.58$, which is incompatible with the observational bound from Cassini $\bar{\alpha} \lesssim 1.7 \times 10^{-3}$ in that mass regime. Since this model does not give rise to Vainshtein screening, we conclude that the β_1 -model is completely ruled out by the combined analysis of cosmological and local data.

Next let us discuss the two-parameter models, which do not give rise to Vainshtein screening as well. This implies that the bounds from local tests of gravity are indeed trustworthy. In fig. 8 we compare the bounds from local and cosmological tests for the two parameter models $\beta_0\beta_1$ and $\beta_1\beta_3$. The blue line defines the boundary of the region that is consistent with cosmological data. The gray-shaded region is excluded by local tests of gravity. For the $\beta_0\beta_1$ -model, cosmological data constrains the spin-2 mass to $m_{\text{FP}} = (1.33 \pm 0.02) \times 10^{-32}$ eV while Cassini constrains the coupling to matter to $\bar{\alpha} \lesssim 1.7 \times 10^{-3}$, which is slightly more stringent than the cosmological bound. For the $\beta_1\beta_n$ -model, the physical parameters are correlated as can be seen in the right panel of fig. 8. Indeed, they are approximately related as $\bar{\alpha}^2 m_{\text{FP}}^2 \simeq \frac{12}{n} \Lambda$ for $n = \{2, 3, 4\}$ (see appendix A.1) [105]. As before, Cassini provides the most stringent constraint on $\bar{\alpha}$. Due to the parameter correlation, this implies a more stringent constraint on the spin-2 mass than inferred from cosmology of $m_{\text{FP}} \gtrsim 1.85 \times 10^{-30}$ eV at 95% c.l. Therefore, all these two-parameter models are in agreement with observational constraints from cosmology and local tests of gravity, but driven to their GR-limits.

In figs. 9 to 11 we combine theoretical, cosmological and local bounds in single plots for all the three parameter models. In all these plots, the regions above the blue lines are excluded at 95% c.l. by our cosmological bounds inferred in section 3.2. The red-shaded regions in the plots are excluded by theoretical constraints that ensure a consistent cosmic expansion history, which we used as hard priors in the cosmological analysis. The region excluded by local bounds at 95% c.l. (if the Vainshtein mechanism is not taken into account) is shown as a gray-shaded region. For large spin-2 masses, the bounds from cosmology are the most stringent ones. For smaller spin-2 masses, the most stringent bound is provided by tests of the scalar curvature with the Cassini spacecraft. Summarising, without taking Vainshtein screening into account, all three-parameter models are consistent with both local tests of gravity and background cosmology. However, since the coupling of the massive spin-2 field to matter is forced to be small, i.e. $\bar{\alpha} \lesssim 1.7 \times 10^{-3}$, all these models are essentially forced into their GR-limits. Although local tests of gravity allow for large couplings to matter if the spin-2 mass is large, $m_{\text{FP}} \gtrsim 10^{-2}$ eV, cosmological data excludes this parameter region. Therefore, deviations from GR are substantially suppressed for these models on all scales.

Let us discuss further about the cosmological bounds on $\bar{\alpha}$ and m_{FP} . From inspecting figs. 9 to 11 we notice that the 95% contour line falls into two regimes. The first is the small spin-2 mass regime. Here, below some critical value that depends on the model, the observational constraints becomes independent of m_{FP} . This is particularly evident for the models with $\beta_0 \neq 0$. In this regime, the coupling to matter $\bar{\alpha}$ is bounded from above as reported in tables 1 and 2. The second regime is above the critical value for m_{FP} , where the contour line can be approximated as:

$$\bar{\alpha}^{c_1} \cdot m_{\text{FP}} \leq 10^{-c_2} \text{ eV}. \quad (4.8)$$

We give the explicit value of the coefficients c_1 and c_2 in table 3, as the result of a polynomial fit. This behavior can be seen in figs. 9 to 11, that however show only a portion of the $\bar{\alpha} - m_{\text{FP}}$ plane scanned by the cosmological analysis¹⁴. Indeed, the approximation (4.8) is valid up to the Planck scale, i.e. beyond the zoomed-in regions in the plots¹⁵.

For the $\beta_1\beta_2\beta_3$ -model, we need to take into account the Vainshtein mechanism when including local tests of gravity. The parameter region, which supports Vainshtein screening, is depicted as a hatched area in the right panel of fig. 10. As we have seen before, the region incorporating Vainshtein screening is almost exactly complementary to the region that is excluded by our theoretical bounds. In particular, the entire parameter region that is consistent with cosmological data gives rise to Vainshtein screening. From the right panel of fig. 10 we see that there is a small overlap between the region excluded by local tests and the region where the Vainshtein mechanism is active. In this interesting region, which is characterized by a potentially large value of $\bar{\alpha}$, local tests are not

¹⁴The wiggles in the contour lines of figs. 9 to 11 are a consequence of zooming in on a portion of the full scanned space, and are interpreted as artifacts of the Markov chains having finite size.

¹⁵The limits on $\bar{\alpha}$ and m_{FP} used in our statistical analysis can be found in section 3.3.

Model	c_1	c_2
$\beta_0\beta_1\beta_4$	0.97 ± 0.01	23.6 ± 0.4
$\beta_0\beta_1\beta_3$	1.117 ± 0.006	32.9 ± 0.2
$\beta_0\beta_1\beta_2$	0.964 ± 0.006	24.6 ± 0.2
$\beta_1\beta_2\beta_3$	1.047 ± 0.007	35.5 ± 0.2
$\beta_1\beta_2\beta_4$	1.021 ± 0.006	32.7 ± 0.2
$\beta_1\beta_3\beta_4$	0.959 ± 0.008	32.7 ± 0.3

Table 3. The value of numerical coefficients for the fitting formula (4.8), obtained with a polynomial fit. We also show 1σ errors in the determination of the coefficients.

trustworthy. Unfortunately this small region seems to be excluded by cosmological data at 95% c.l. in our statistical analysis. However, this is probably caused by prior domination. Indeed, this is a very small region of the full parameter space explored by the statistical analysis and it is close to the hard prior given by the theoretical constraints. To further investigate this issue, one should perform another statistical analysis focusing on this small region of parameter space.

For the models with $\beta_0 = 0$, the 95% contour lies very close to the theoretical priors except for a few wiggles. We interpret the wiggles as an artifact of the finite size of the Markov chains and conclude that the used data sets are not constraining these parameters. Instead, the statistically favored regions almost exactly coincide with the parameter regions allowed by our theoretical priors. To stabilise the value of $\bar{\alpha}$ and m_{FP} , we would need to include other data sets, which however is beyond the scope of the present analysis.

On the other hand, models with $\beta_4 = 0$ are subject to rather weak theoretical priors. Nonetheless, the 95% lines show the same tendency as for the other models. Hence, the data sets constrain these parameters substantially beyond the prior knowledge, but is not able to stabilise their values. To understand why the upper-right region in the $\bar{\alpha} - m_{\text{FP}}$ -plane is excluded also for these models, we note the following. Expanding the expression for β_0 in the limit $m_{\text{FP}}^2 \gg \Lambda$, we find that $\beta_0 \simeq -\frac{12}{n}\bar{\alpha}^2 m_{\text{FP}}^2$ for the $\beta_0\beta_1\beta_n$ -model with $n = \{2, 3, 4\}$. This allows to conclude that data disfavors large negative values of β_0 . This means that, in order to be cosmologically viable, ρ_{de} is allowed to change its sign only at sufficiently large redshifts.

5 Conclusions and outlook

Massive spin-2 fields might play a crucial role in our universe. Their (self-)interaction energy can drive the observed cosmic accelerated expansion at late times. Furthermore, a massive spin-2 field serves as ideal dark matter candidate as it interacts with ordinary matter only gravitationally [84–86]. Recently, another intriguing aspect has been explored within a completely different context. As argued in [163], massive spin-2 states could be essential in solving the black hole information paradoxon.

In this paper, we have further studied the observational viability of bimetric theory. We confronted all models with up to three free interaction parameters β_n with measurements of SN1a, BAOs and CMB. We find that all two and three parameter models are in perfect agreement with these data sets. Compared to the Λ CDM model, bimetric models are statistically disfavored due to the larger number of free parameters. However, the self-accelerating solutions with $\beta_0 = 0$ appear more appealing from a theoretical perspective as these models do not suffer the cosmological constant problems [12, 13].

The best-fit values for the cosmological parameters do not significantly differ from the best-fit values of the Λ CDM model. We have also studied spatial curvature within bimetric theory, and our results show that a spatially flat universe is always preferred.

The only exception from the previous summary is the β_1 -model, which represents the simplest bimetric model that gives rise to self-accelerating solutions on the finite branch. Our statistical analysis shows that the aforementioned data sets are inconsistent leading to a substantially higher

χ^2 at the best fit point. We therefore conclude that the β_1 -model is statistically disfavored. This conclusion is further strengthened when simultaneously confronting this model with local tests of gravity. Cosmological data selects a spin-2 mass of $m_{\text{FP}} = (1.82 \pm 0.02) \times 10^{-32}$ eV, for which local tests of gravity demand a coupling to matter of $\bar{\alpha} \lesssim 1.7 \times 10^{-3}$ at 95% c.l. Within the β_1 -model, this parameter is fixed to be $\bar{\alpha} = 3^{-1/2}$. Therefore, this model is in severe conflict with observations.

We also analysed the other bimetric models with up to three free parameters, for which we compared the bounds from background cosmology to the ones obtained from local tests of gravity. All models are consistent with both types of observations even if the Vainshtein mechanism is not active. However, the coupling of the massive spin-2 field to ordinary matter is forced to be small, $\bar{\alpha} \lesssim 10^{-3}$ (see section 4.1 and tables 1 and 2 for the precise values). For large spin-2 masses, the cosmological observations force the coupling to be even smaller. This suppresses the deviations from GR on all scales for these models.

For the $\beta_1\beta_2\beta_3$ -model, the Vainshtein mechanism removes the constraint on $\bar{\alpha}$ and m_{FP} implied by local tests for sufficiently small values of the spin-2 mass. In this region, where $\bar{\alpha}$ can be large, the theory is not in its GR limit. As we mentioned in section 4.3, the fact that this small region is excluded by our cosmological analysis might be a numerical effect, and it would be interesting to further investigate this issue in another analysis. Further, more general bimetric models, i.e. those with four or all five parameters β_n being free, might not be forced into their GR-limits. In any case, even if the restricted models studied in this paper turn out to be forced into their GR-limits, their theoretical motivation would persist: self-accelerating models with $\beta_0 = 0$ have an effective cosmological constant that is technical natural in the sense of t’Hooft [164].

The data sets used in this paper are only weakly constraining the physical parameter space of $\bar{\alpha}$ and m_{FP} . To stabilise their values and effectively constrain bimetric theories, a possibility would be taking into account further measurements. Cosmological perturbations around the FLRW background solution are expected to have constraining power as these probe different redshifts and scales. However, in bimetric theory linear scalar perturbations are plagued by gradient instabilities at early times [65, 70, 74, 77–79]. The instability sets in when the Hubble rate is of the order of the spin-2 mass, $H \simeq m_{\text{FP}}$ [69]. Nonlinear terms become as important as the linear term rendering perturbation theory invalid. Indeed, taking nonlinearities into account might stabilise the solution in analogy to the Vainshtein mechanism [69, 81, 82, 128]. Structure formation and nonlinear cosmological perturbations are therefore main open issues within bimetric theory, which should be addressed in the future.

Acknowledgements

We thank Marcus Högås and Edvard Mörtzell for interesting discussions and useful comments on the manuscript. We are grateful to Thomas Hahn, Martin Kerscher and Kerstin Paech for their kind help regarding the statistical analysis and numerical implementation. We further acknowledge the usage of the `Getdist` package, which we extensively used for the statistical analysis [165]. The work of ML is supported by a grant from the Max Planck Society. The work of AC and JW is supported by the Excellence Cluster ORIGINS which is funded by the Deutsche Forschungsgemeinschaft (DFG, German Research Foundation) under Germany’s Excellence Strategy - EXC-2094 - 390783311.

A Details on the physical parametrisation

In order to provide an overview over the relation between the physical and interaction parameters, we summarise the results of Ref. [105] in this appendix. We immediately work in terms of the cosmological parameters that we use for parameter fitting.

In the β_1 -model, there is only one free physical parameter, in terms of which the interaction parameter is given as

$$B_1 = \frac{1}{\sqrt{3}}\Omega_\Lambda = \frac{\sqrt{3}}{4}\Omega_{\text{FP}}, \quad (\text{A.1})$$

while the mixing angle is fixed to be $\bar{\alpha} = 1/\sqrt{3}$.

A.1 Two-parameter models

Next, we turn to the two-parameter models with $\beta_1 \neq 0$. We choose to express the interaction parameters on terms of Ω_{FP} and Ω_Λ , while the mixing angle $\bar{\alpha}$ is a derived parameter. However, one can equivalently eliminate one of the physical parameters by $\bar{\alpha}$. For the $\beta_0\beta_1$ -model, the relation between the parameters is

$$B_0 = -3\Omega_{\text{FP}} + 4\Omega_\Lambda, \quad B_1 = \sqrt{(\Omega_{\text{FP}} - \Omega_\Lambda)\Omega_\Lambda}, \quad (\text{A.2})$$

in terms of which the mixing angle is determined to be $\bar{\alpha} = \sqrt{\Omega_{\text{FP}}/\Omega_\Lambda - 1}$.

For the $\beta_1\beta_2$ -model, the relation is given by

$$\begin{aligned} B_1 &= \frac{1}{2} \sqrt{\frac{3\Omega_{\text{FP}} - 2\Omega_\Lambda - \Delta_{12}}{3\Omega_\Lambda}} (3\Omega_{\text{FP}} - 3\Omega_\Lambda + \Delta_{12}), \\ B_2 &= -\frac{1}{6} (3\Omega_{\text{FP}} - 5\Omega_\Lambda + \Delta_{12}) \end{aligned} \quad (\text{A.3})$$

where we defined $\Delta_{12} = \sqrt{9\Omega_{\text{FP}}^2 - 12\Omega_{\text{FP}}\Omega_\Lambda + \Omega_\Lambda^2}$. The mixing angle is given by $\bar{\alpha}^2 = (3\Omega_{\text{FP}} - 2\Omega_\Lambda - \Delta_{12})/(3\Omega_\Lambda)$. To avoid numerical instabilities, it is convenient to expand the expressions for $\Omega_{\text{FP}} \gg \Omega_\Lambda$. In this limit, the parameter relation reads

$$\bar{\alpha} \simeq \sqrt{\frac{\Omega_\Lambda}{6\Omega_{\text{FP}}}}, \quad B_1 \simeq \sqrt{\frac{3\Omega_{\text{FP}}\Omega_\Lambda}{2}}, \quad B_2 \simeq -\Omega_{\text{FP}}. \quad (\text{A.4})$$

Next, we turn to the $\beta_1\beta_3$ -model, where the relations read

$$B_1 = \frac{1}{4} \sqrt{\frac{2\Omega_{\text{FP}} - \Omega_\Lambda - 2\Delta_{13}}{\Omega_\Lambda}} \sqrt{3\Omega_{\text{FP}} - 2\Omega_\Lambda + 3\Delta_{13}}, \quad (\text{A.5})$$

$$B_3 = -\sqrt{\frac{2\Omega_{\text{FP}} - \Omega_\Lambda - 2\Delta_{13}}{\Omega_\Lambda}} (4\Omega_{\text{FP}}^2 - 7\Omega_{\text{FP}}\Omega_\Lambda + 2\Omega_\Lambda^2 + \Delta_{13}(4\Omega_{\text{FP}} - 5\Omega_\Lambda)). \quad (\text{A.6})$$

with $\Delta_{13} = \sqrt{(\Omega_{\text{FP}} - \Omega_\Lambda)\Omega_{\text{FP}}}$. The mixing angle is given by $\bar{\alpha}^2 = (2\Omega_{\text{FP}} - \Omega_\Lambda - 2\Delta_{13})/(\Omega_\Lambda)$. Again, to avoid numerical instabilities, we expand the expressions for $\Omega_{\text{FP}} \gg \Omega_\Lambda$ yielding

$$\bar{\alpha} \simeq \frac{1}{2} \sqrt{\frac{\Omega_\Lambda}{\Omega_{\text{FP}}}}, \quad B_1 \simeq \frac{3}{4} \sqrt{\Omega_{\text{FP}}\Omega_\Lambda}, \quad B_3 \simeq -\sqrt{\frac{\Omega_{\text{FP}}^3}{\Omega_\Lambda}}. \quad (\text{A.7})$$

Finally, in the $\beta_1\beta_4$ -model the parameter relations read

$$B_1 = \frac{1}{3} \sqrt{(3\Omega_{\text{FP}} - \Omega_\Lambda)\Omega_\Lambda}, \quad (\text{A.8})$$

$$B_4 = -\frac{9\Omega_{\text{FP}}^2 - 15\Omega_{\text{FP}}\Omega_\Lambda + 4\Omega_\Lambda^2}{3\Omega_\Lambda} \quad (\text{A.9})$$

while the mixing angle reads $\bar{\alpha}^2 = \Omega_\Lambda/(3\Omega_{\text{FP}} - \Omega_\Lambda)$.

A.2 Three-parameter models

We continue by stating the parameter relations for the three-parameter models with $\beta_1 \neq 0$. For the $\beta_0\beta_1\beta_2$ -model, the relations read

$$\begin{aligned} B_0 &= -\frac{6\bar{\alpha}^2\Omega_{\text{FP}} - (1 + 4\bar{\alpha}^2 + 3\bar{\alpha}^4)\Omega_\Lambda}{1 + \bar{\alpha}^2}, \\ B_1 &= \bar{\alpha} \left(\frac{3\Omega_{\text{FP}}}{1 + \bar{\alpha}^2} - 2\Omega_\Lambda \right) \\ B_2 &= -\frac{\Omega_{\text{FP}}}{1 + \bar{\alpha}^2} + \Omega_\Lambda. \end{aligned} \quad (\text{A.10})$$

Model	Viable cosmology	Vainshtein screening
$\beta_0\beta_1$	$\Omega_{\text{FP}} > \Omega_\Lambda$	–
$\beta_1\beta_2$	$3\Omega_{\text{FP}} > (2 + \sqrt{3})\Omega_\Lambda$	–
$\beta_1\beta_3$	$\Omega_{\text{FP}} > \Omega_\Lambda$	–
$\beta_0\beta_1\beta_2$	$3\Omega_{\text{FP}} > 2(1 + \bar{\alpha}^2)\Omega_\Lambda$	–
$\beta_0\beta_1\beta_3$	$4\Omega_{\text{FP}} > (1 + \bar{\alpha}^2)^2\Omega_\Lambda$	–
$\beta_1\beta_2\beta_3$	$4\bar{\alpha}^4\Omega_{\text{FP}} < (1 + \bar{\alpha}^2)^2\Omega_\Lambda$ $6\bar{\alpha}^2\Omega_{\text{FP}} < (3 + 4\bar{\alpha}^2 + \bar{\alpha}^4)\Omega_\Lambda$	$16\bar{\alpha}^2\Omega_{\text{FP}} \lesssim \Omega_\Lambda$
$\beta_1\beta_2\beta_4$	$3\bar{\alpha}^2\Omega_{\text{FP}} < 2(1 + \bar{\alpha}^2)\Omega_\Lambda$ $3\bar{\alpha}^4\Omega_{\text{FP}} < (1 + \bar{\alpha}^2)^2\Omega_\Lambda$	–
$\beta_1\beta_3\beta_4$	$\bar{\alpha}^2\Omega_{\text{FP}} < (1 + \bar{\alpha}^2)\Omega_\Lambda$	–

Table 4. This table summarises the theoretical constraints on all bimetric models with up to three non-vanishing interaction parameters. The cosmology constraints were derived in Ref. [105] and follow from requiring a consistent cosmic expansion history. We only state the most stringent constraints other than the Higuchi bound, $3\Omega_{\text{FP}} > 2\Omega_\Lambda$. Only the $\beta_1\beta_2\beta_3$ -model has a working Vainshtein mechanism. We report the approximation of the most stringent bound.

In the $\beta_0\beta_1\beta_3$ -model, the physical and interaction parameters are related as

$$\begin{aligned}
B_0 &= -\frac{4\bar{\alpha}^2\Omega_{\text{FP}} - (1 + 2\bar{\alpha}^2 + \bar{\alpha}^4)\Omega_\Lambda}{1 + \bar{\alpha}^2}, \\
B_1 &= \frac{\bar{\alpha}}{2} \left(\frac{3\Omega_{\text{FP}}}{1 + \bar{\alpha}^2} - \Omega_\Lambda \right), \\
B_3 &= -\frac{1}{2\bar{\alpha}} \left(\frac{\Omega_{\text{FP}}}{1 + \bar{\alpha}^2} - \Omega_\Lambda \right).
\end{aligned} \tag{A.11}$$

Next, the $\beta_0\beta_1\beta_4$ -model gives rise to the following relations,

$$B_0 = -\frac{3\bar{\alpha}^2\Omega_{\text{FP}}}{1 + \bar{\alpha}^2} + \Omega_\Lambda, \quad B_1 = \frac{\bar{\alpha}\Omega_{\text{FP}}}{1 + \bar{\alpha}^2}, \quad B_4 = -\frac{1}{\bar{\alpha}^2} \left(\frac{\Omega_{\text{FP}}}{1 + \bar{\alpha}^2} - \Omega_\Lambda \right). \tag{A.12}$$

Turning to models with $\beta_0 = 0$, the parameter relations for the $\beta_1\beta_2\beta_3$ -model read

$$\begin{aligned}
B_1 &= \frac{-6\bar{\alpha}^2\Omega_{\text{FP}} + (3 + 4\bar{\alpha}^2 + \bar{\alpha}^4)\Omega_\Lambda}{4\bar{\alpha}(1 + \bar{\alpha}^2)}, \\
B_2 &= \frac{4\bar{\alpha}^2\Omega_{\text{FP}} - (1 + 2\bar{\alpha}^2 + \bar{\alpha}^4)\Omega_\Lambda}{2\bar{\alpha}^2(1 + \bar{\alpha}^2)}, \\
B_3 &= -\frac{6\bar{\alpha}^2\Omega_{\text{FP}} - (1 + 4\bar{\alpha}^2 + 3\bar{\alpha}^4)\Omega_\Lambda}{4\bar{\alpha}^3(1 + \bar{\alpha}^2)}.
\end{aligned} \tag{A.13}$$

Next, the $\beta_1\beta_2\beta_4$ -model has the following parameter relations,

$$\begin{aligned}
B_1 &= \frac{-3\bar{\alpha}^2\Omega_{\text{FP}} + 2(1 + \bar{\alpha}^2)\Omega_\Lambda}{3\bar{\alpha}(1 + \bar{\alpha}^2)}, \\
B_2 &= \frac{3\bar{\alpha}^2\Omega_{\text{FP}} - (1 + \bar{\alpha}^2)\Omega_\Lambda}{3\bar{\alpha}^2(1 + \bar{\alpha}^2)}, \\
B_4 &= -\frac{6\bar{\alpha}^2\Omega_{\text{FP}} - (1 + 4\bar{\alpha}^2 + 3\bar{\alpha}^4)\Omega_\Lambda}{3\bar{\alpha}^4(1 + \bar{\alpha}^2)}.
\end{aligned} \tag{A.14}$$

Finally, in the $\beta_1\beta_3\beta_4$ -model the interaction and physical parameters are related as

$$\begin{aligned} B_1 &= \frac{-\bar{\alpha}^2\Omega_{\text{FP}} + (1 + \bar{\alpha}^2)\Omega_\Lambda}{2\bar{\alpha}(1 + \bar{\alpha}^2)}, \\ B_3 &= \frac{3\bar{\alpha}^2\Omega_{\text{FP}} - (1 + \bar{\alpha}^2)\Omega_\Lambda}{2\bar{\alpha}^3(1 + \bar{\alpha}^2)}, \\ B_4 &= \frac{-4\bar{\alpha}^2\Omega_{\text{FP}} + (1 + 2\bar{\alpha}^2 + \bar{\alpha}^4)\Omega_\Lambda}{\bar{\alpha}^4(1 + \bar{\alpha}^2)}. \end{aligned} \quad (\text{A.15})$$

B Vainshtein screening in static, spherically symmetric systems

In this appendix, we will solve the bimetric equations of motion for the static, spherically symmetric, and bidiagonal ansatz. This allows to study the Vainshtein mechanism in these systems, which restores General Relativity on small length scales. However, a solution that incorporates the Vainshtein mechanism does not exist for every set of bimetric parameters. Instead, demanding existence of such a solution implies conditions on the bimetric parameters. The situation was studied in detail in Refs. [90, 93] however with flat asymptotics. We aim at generalizing the analysis allowing for a non-zero cosmological constant [166] and compute the conditions for the Vainshtein mechanism to work in this more general setup. As we will see, our results reduce to the ones of Ref. [90, 93] in the limit of vanishing cosmological constant.

Assuming staticity and spherical symmetry, the metrics $g_{\mu\nu}$ and $f_{\mu\nu}$ can be written in the bidiagonal case as [93]

$$\begin{aligned} ds_g^2 &= -e^{-\nu_g} dt^2 + e^{\lambda_g} dr^2 + r^2 d\Omega^2, \\ ds_f^2 &= -e^{-\nu_f} dt^2 + e^{\lambda_f} (r + r\mu)^2 dr^2 + (r + r\mu)^2 d\Omega^2. \end{aligned} \quad (\text{B.1})$$

The metric functions $\nu_{g,f}$, $\lambda_{g,f}$, and μ depend on radius r only. The field μ can be thought of as a Stückelberg field that restores diffeomorphisms in the r -dimension.

First, let us introduce the following short-hand notation,

$$\beta = \frac{1 + \bar{\alpha}^2}{\bar{\alpha}^2 m_{\text{FP}}^2} c^2 (\beta_2 + \beta_3 c), \quad \gamma = \frac{1 + \bar{\alpha}^2}{\bar{\alpha}^2 m_{\text{FP}}^2} c^3 \beta_3. \quad (\text{B.2})$$

To simplify the equation of motion, we assume that the gravitational fields and their derivatives are small, $\{\lambda_{g,f}, \nu_{g,f}\} \ll 1$ and $\{r\lambda'_{g,f}, r\nu'_{g,f}\} \ll 1$, but we keep all nonlinearities in μ . This results in the following set of Einstein equation for $g_{\mu\nu}$,

$$\begin{aligned} \frac{(r\lambda_g)'}{r^2} &= \Lambda + \frac{\rho(r)}{m_g^2} + \frac{\bar{\alpha}^2 m_{\text{FP}}^2}{1 + \bar{\alpha}^2} \left(\frac{1}{2} (\lambda_f - \lambda_g) + \frac{1}{r^2} \left[r^3 \left(\mu + \beta\mu^2 + \frac{\gamma}{3}\mu^3 \right) \right]' \right) \\ \frac{\lambda_g}{r^2} - \frac{\nu_g'}{r} &= \Lambda + \frac{\bar{\alpha}^2 m_{\text{FP}}^2}{1 + \bar{\alpha}^2} \left(\frac{1}{2} (\nu_f - \nu_g) + 2\mu + \beta\mu^2 \right), \\ -\frac{\lambda_g'}{2r} + \frac{(r\nu_g')'}{2r} &= \Lambda + \frac{\bar{\alpha}^2 m_{\text{FP}}^2}{1 + \bar{\alpha}^2} \left(\frac{1}{2} (\lambda_f - \lambda_g + \nu_f - \nu_g) + \frac{1}{r} \left[r^2 \left(\mu + \frac{\beta}{2}\mu^2 \right) \right]' \right). \end{aligned} \quad (\text{B.3})$$

With the same approximations, the Einstein equations of $f_{\mu\nu}$ can be arranged to

$$\begin{aligned} \frac{((r + r\mu)\lambda_f)'}{r^2} &= \Lambda - \frac{m_{\text{FP}}^2}{1 + \bar{\alpha}^2} \left(\frac{1}{2} (\lambda_f - \lambda_g) + \frac{1}{r^2} \left[r^3 \left(\mu + (1 + \beta)\mu^2 + \frac{1 + \beta + \gamma}{3}\mu^3 \right) \right]' \right), \\ (r + r\mu)' \frac{\lambda_f}{r^2} - (1 + \mu) \frac{\nu_f'}{r} &= \Lambda - \frac{m_{\text{FP}}^2}{1 + \bar{\alpha}^2} \left(\frac{1}{2} (\nu_f - \nu_g) + 2\mu + (1 + \beta)\mu^2 \right) (r + r\mu)', \\ \frac{\lambda_f}{2r} - \frac{1}{2r} \left(\frac{(r + r\mu)\nu_f'}{(r + r\mu)'} \right)' &= \Lambda - \frac{m_{\text{FP}}^2}{1 + \bar{\alpha}^2} \left(\frac{1}{2} (\lambda_f - \lambda_g - \nu_f - \nu_g) + \frac{1}{r} \left[r^2 \left(\mu + \frac{1 + \beta}{2}\mu^2 \right) \right]' \right) \end{aligned} \quad (\text{B.4})$$

Note that we do not present the $\phi\phi$ -components of the Einstein equations as these coincide with the $\theta\theta$ -components. The last ingredient is the Bianchi constraint, that simplifies to

$$\frac{(r+r\mu)'}{r}(1+\beta\mu)(\lambda_f-\lambda_g)-\frac{1}{2}(1+2\beta\mu+\gamma\mu^2)(\nu_f'-(r+r\mu)'\nu_g')=0. \quad (\text{B.5})$$

Even in this simplified approximation, the equations are not solvable analytically. To find analytic solutions, we will go to large radii where all metric functions and their derivatives have to be small because we assume spacetime to be asymptotically de Sitter while remaining far inside the de Sitter horizon $3/\sqrt{\Lambda}$. The other limit is for small radii compared to the Compton wavelength of the massive spin-2 field.

B.1 Approximate solutions

B.1.1 Linear regime

First, we will solve the equations of motion for $r \gg r_S$ with r_S the Schwarzschild radius of a localised source to be defined later. For large radii smaller than the de Sitter horizon, all metric functions, including μ , are assumed to be small such that both metrics approach de Sitter solution asymptotically. We expand the Einstein equations and the Bianchi constraint further in $\mu \ll 1$ and $r\mu' \ll 1$. It is convenient to introduce the auxiliary functions,

$$\lambda_{\pm} = \lambda_f \pm \lambda_g, \quad \nu_{\pm} = \nu_f \pm \nu_g \quad (\text{B.6})$$

In terms of these functions, the linearised Bianchi constraint (B.5) reads,

$$2\lambda_- = r\nu'_-, \quad (\text{B.7})$$

which is independent of the $+$ -fields. We can find linear combinations of the Einstein equations for $g_{\mu\nu}$ and $f_{\mu\nu}$ such that the $+$ -fields drop out of the expression,

$$\begin{aligned} 0 &= 2r\lambda'_- + (2 + m_{\text{FP}}^2 r^2) \lambda_- + 2m_{\text{FP}}^2 r^2 (3\mu + r\mu'), \\ 0 &= -2\lambda_- + m_{\text{FP}}^2 r^2 (\nu_- + 4\mu), \\ 0 &= r\lambda'_- - m_{\text{FP}}^2 r^2 (\lambda_- + \nu_- + 4\mu + 2r\mu'), \end{aligned} \quad (\text{B.8})$$

where we have used the Bianchi constrained already to eliminate ν'_- and ν''_- in terms of λ_- and λ'_- . The equations reduce to two coupled differential equations for λ_- and μ ,

$$\lambda'_- = -2m_{\text{FP}}^2 r\mu, \quad \mu' = -\frac{(2 + m_{\text{FP}}^2 r^2)\lambda_- + 2m_{\text{FP}}^2 r^2 \mu}{2m_{\text{FP}}^2 r^3}, \quad (\text{B.9})$$

while ν_- is algebraically determined by the other two fields. These equations are solved by

$$\begin{aligned} \nu_- &= \frac{C_1 e^{-m_{\text{FP}} r}}{r}, \\ \lambda_- &= -\frac{C_1 (1 + m_{\text{FP}} r) e^{-m_{\text{FP}} r}}{2r}, \\ \mu &= -\frac{C_1 (1 + m_{\text{FP}} r + m_{\text{FP}}^2 r^2) e^{-m_{\text{FP}} r}}{4m_{\text{FP}}^2 r^3}, \end{aligned} \quad (\text{B.10})$$

where C_1 is a constant of integration to be determined later. We already fixed the other constant of integration by requiring that the fields vanish in the limit $r \rightarrow \infty$ in order to ensure that the metrics are asymptotically bidiagonal and de Sitter. Next, we turn to the other set of linearly independent equations that contain also the $+$ -fields. These can be arranged to

$$\begin{aligned} 0 &= (\bar{\alpha}^2 - 1)(\lambda_- + r\lambda'_-) + (1 + \bar{\alpha}^2)(\lambda_+ + r\lambda'_+) - 2(1 + \bar{\alpha}^2)\Lambda r^2, \\ 0 &= (\bar{\alpha}^2 - 1)\lambda_- - (1 + \bar{\alpha}^2)(\lambda_+ - r\nu'_+) + 2(1 + \bar{\alpha}^2)\Lambda r^2, \\ 0 &= (\bar{\alpha}^2 - 1)\lambda'_- - (1 + \bar{\alpha}^2)(\lambda'_+ - \nu'_+ - r\nu''_+ - 4\Lambda r) \end{aligned} \quad (\text{B.11})$$

Upon using eq. (B.10), these equations are solved by

$$\begin{aligned}\nu_+ &= -\frac{2\Lambda r^2}{3} - \frac{2C_2}{r} - \frac{C_1 e^{-m_{\text{FP}} r}}{(1 + \bar{\alpha}^2)r}, \\ \lambda_+ &= \frac{2\Lambda r^2}{3} + \frac{2C_2}{r} + \frac{C_1(1 + m_{\text{FP}} r)e^{-m_{\text{FP}} r}}{2(1 + \bar{\alpha}^2)r},\end{aligned}\tag{B.12}$$

where C_2 is another constant of integration. Again, we have already used that the functions have to be bidiagonal and de Sitter in the limit $r \rightarrow \infty$ to fix one of the constants of integration. Having solved the differential equations for all the fields, we can present the final solutions for the metric fields in the linearised limit. They are given by

$$\begin{aligned}\mu &= -\frac{C_1(1 + m_{\text{FP}} r + m_{\text{FP}}^2 r^2)e^{-m_{\text{FP}} r}}{4m_{\text{FP}}^2 r^3}, \\ \nu_{\text{g}} &= -\frac{\Lambda r^2}{3} - \frac{C_2}{r} - \frac{C_1 \bar{\alpha}^2 e^{-m_{\text{FP}} r}}{(1 + \bar{\alpha}^2)r}, \\ \nu_{\text{f}} &= -\frac{\Lambda r^2}{3} - \frac{C_2}{r} + \frac{C_1 e^{-m_{\text{FP}} r}}{(1 + \bar{\alpha}^2)r}, \\ \lambda_{\text{g}} &= \frac{\Lambda r^2}{3} + \frac{C_2}{r} + \frac{C_1 \bar{\alpha}^2 (1 + m_{\text{FP}} r)e^{-m_{\text{FP}} r}}{2(1 + \bar{\alpha}^2)r}, \\ \lambda_{\text{f}} &= \frac{\Lambda r^2}{3} + \frac{C_2}{r} - \frac{C_1(1 + m_{\text{FP}} r)e^{-m_{\text{FP}} r}}{2(1 + \bar{\alpha}^2)r}.\end{aligned}\tag{B.13}$$

In the limit of a vanishing cosmological constant, $\Lambda = 0$, our linearised solutions reduce to the results obtained in Refs. [90, 93].

Let us comment on the region of validity of these solutions. As we will see later, $C_1 \sim r_{\text{S}}$. Hence, all metric fields are small on scales $r \gg r_{\text{S}}$ and inside the de Sitter horizon, $r \ll \Lambda^{-1/2}$. This is not true however for the Stückelberg field μ , which is small only on scales $r \gg (r_{\text{S}}/m_{\text{FP}}^2)^{1/3}$. In general, this scale is larger than the Schwarzschild radius of the source. These solutions are hence not appropriate to describe the scales $r_{\text{S}} \ll r \ll (r_{\text{S}}/m_{\text{FP}}^2)^{1/3}$. In the next section, we seek solutions that are valid on these scales.

B.1.2 Compton regime

Next, we want to solve the equations on scales much smaller than the Compton wavelength of the massive spin-2 field, i.e. for $r \ll m_{\text{FP}}^{-1}$. Technically that means that we omit the terms $m_{\text{FP}}^2 r^2 \cdot \{\lambda_{\text{g,f}}, \nu_{\text{g,f}}\} \ll 1$ in the modified Einstein equations.

Under this approximation we can integrate the tt -component of eq. (B.3) to

$$\lambda_{\text{g}} = \frac{r_{\text{S}}}{r} + \frac{\bar{\alpha}^2 m_{\text{FP}}^2 r^2}{1 + \bar{\alpha}^2} \left(\mu + \beta \mu^2 + \frac{\gamma}{3} \mu^3 \right),\tag{B.14}$$

where we defined the Schwarzschild radius

$$r_{\text{S}} = \frac{1}{4\pi m_{\text{g}}^2} \int_0^{R_*} \rho r^2 dr\tag{B.15}$$

of a source of mass M and radius R_* . The solution is valid outside the compact object and we fixed the constants of integration by demanding regularity at the surface of the compact object and at the origin $r = 0$. Upon using the solution for λ_{g} , the rr -component of eq. (B.3) simplifies to

$$r\nu'_{\text{g}} = \frac{r_{\text{S}}}{r} - \frac{\bar{\alpha}^2 m_{\text{FP}}^2 r^2}{1 + \bar{\alpha}^2} \left(\mu - \frac{\gamma}{3} \mu^3 \right).\tag{B.16}$$

The tt -component of eq. (B.4) can easily be integrated to

$$\lambda_f = -\frac{m_{\text{FP}}^2}{1+\bar{\alpha}^2} \frac{r^2}{1+\mu} \left(\mu + (1+\beta)\mu^2 + \frac{1+\beta+\gamma}{3}\mu^3 \right). \quad (\text{B.17})$$

Here, we fixed the constant of integration by demanding regularity at the origin $r = 0$. With this result, the rr -component of eq. (B.3) simplifies to

$$r\nu'_f = \frac{m_{\text{FP}}^2}{1+\bar{\alpha}^2} \frac{r^2(r+r\mu)'}{(1+\mu)^2} \left(\mu + 2\mu^2 + \frac{2+2\beta-\gamma}{3}\mu^3 \right). \quad (\text{B.18})$$

We have obtained expression for all the fields that show up in the Bianchi constraint in terms of μ . Plugging these results into the Bianchi constraint yields the following algebraic polynomial for μ :

$$\begin{aligned} & -3(3+3\bar{\alpha}^2)\mu \\ & -2(9(1+\bar{\alpha}^2)(1+\beta))\mu^2 \\ & - (10+9\bar{\alpha}^2+2(17+18\bar{\alpha}^2)\beta+6(1+\bar{\alpha}^2)\beta^2+4(1+\bar{\alpha}^2)\gamma)\mu^3 \\ & -2(1+(7+9\bar{\alpha}^2)\beta+6(1+\bar{\alpha}^2)\beta^2+4(1+\bar{\alpha}^2)\gamma)\mu^4 \\ & - (2(1+2\gamma)\beta+2(1+3\bar{\alpha}^2)\beta^2+2(1+2\bar{\alpha}^2)\gamma-(1+\bar{\alpha}^2)\gamma^2)\mu^5 \\ & +2\bar{\alpha}^2\gamma^2\mu^6+\bar{\alpha}^2\gamma^2\mu^7 \\ & = 3\left(\frac{r_V}{r}\right)^3(1+\bar{\alpha}^2)(1+\mu)^2(1-\gamma\mu^2). \end{aligned} \quad (\text{B.19})$$

In here, we defined the Vainshtein radius

$$r_V = \left(\frac{r_S}{m_{\text{FP}}^2} \right)^{1/3} \quad (\text{B.20})$$

that we already encountered before. Our result coincides with the one obtained in Ref. [90].

Eq. (B.19) represents a seventh order algebraic polynomial for μ and as such has up to seven solutions. As argued in Ref. [93] for $\gamma > 0$, three solutions are real-valued for all r , while two solutions are real only up to a certain critical radius that depends on the other parameters. The last two solutions are complex-valued. The three everywhere real-valued solutions are shown in Fig. 12. In the opposite case $\gamma < 0$, two of the real-valued solutions become complex-valued and the remaining real-valued solutions are neither asymptotically bidiagonal nor restore GR inside the Vainshtein regime. The case $\gamma = 0$ is special because the polynomial is only of degree five. There is one solution that realises the Vainshtein mechanism for small radii, which however is not asymptotically bidiagonal and it is complex-valued for very small radii. Although there might be special situations in which the Vainshtein mechanism works even for this case [93, 160], we exclude $\gamma = 0$ from our analysis and restrict to $\gamma > 0$.

We can infer further information about the general behavior of μ . For radii much larger than the Vainshtein radius, the term $(r_V/r)^3$ on the right hand side of eq. (B.19) is small, which implies that the Stückelberg field is small as well, $\mu \ll 1$. This gives rise to three asymptotic values for μ as can be seen in Fig. 12. One of these is given by $\mu = 0$ such that we can neglect nonlinearities in μ . This solution corresponds to the one obtained when linearising the field equations as in appendix B.1.1. For small radii, the term $(r_V/r)^3$ on the right hand side is large. This allows to identify two classes of solutions. Either, μ on the right hand side compensates that large term. This is the case for $\mu = -1$ or $\mu = \pm 1/\sqrt{\gamma}$. Note that the second solution exists only for $\gamma > 0$. These are the three asymptotic values that show up in Fig. 12. The other possibility is that μ diverges as $r \rightarrow 0$.

B.1.3 Matching the analytic solutions

It remains to determine the constants of integration C_1 and C_2 . We do this by matching the analytic solutions in the regime where both of them are valid, i.e. $r_V \ll r \ll m_{\text{FP}}^{-1}$. Linearising the nonlinear

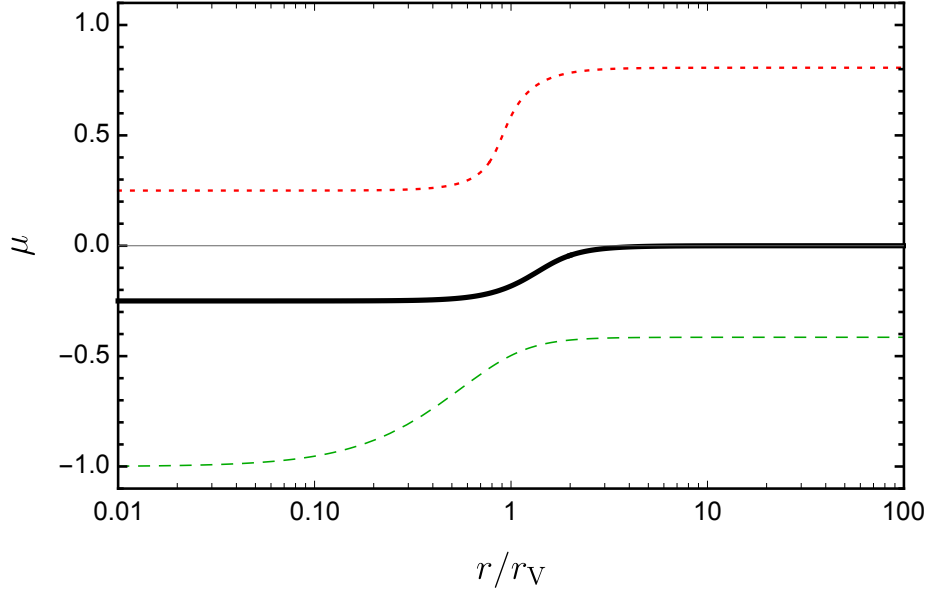


Figure 12. Plot of the Stückelberg field μ as a function of r/r_V for the exemplary parameter values $\bar{\alpha} = 1$, $\beta = 1$, and $\gamma = 16$. The Vainshtein-Yukawa solution (solid black) smoothly evolves from zero at large distances to a non-zero value inside the Vainshtein regime such as to restore GR on these scales. The other two solutions (red dotted and green dashed) also restore GR inside the Vainshtein regime, but they do not tend to zero asymptotically. For the same set of parameters, there are two more solutions that are real valued only for small radii r .

solutions eqs. (B.14), (B.17) and (B.19) for $r \gg r_V$, we obtain

$$\mu = -\frac{r_S}{3m_{\text{FP}}^2 r^3}, \quad \lambda_g = \frac{(3 + 2\bar{\alpha}^2)r_S}{3(1 + \bar{\alpha}^2)r}, \quad \lambda_f = \frac{r_S}{3(1 + \bar{\alpha}^2)r}. \quad (\text{B.21})$$

Here, we linearised the Stückelberg field around $\mu = 0$. Expanding on the other hand the linear solutions (B.13) for $r \ll m_{\text{FP}}^{-1}$ yields

$$\mu = -\frac{C_1}{4m_{\text{FP}}^2 r^3}, \quad \lambda_g = \frac{\bar{\alpha}^2 C_1 + 2(1 + \bar{\alpha}^2)C_2}{2(1 + \bar{\alpha}^2)r}, \quad \lambda_f = -\frac{C_1 - 2(1 + \bar{\alpha}^2)C_2}{2(1 + \bar{\alpha}^2)r}. \quad (\text{B.22})$$

These solutions coincide, if we choose the constants of integration to be

$$C_1 = \frac{4r_S}{3}, \quad C_2 = \frac{r_S}{1 + \bar{\alpha}^2}. \quad (\text{B.23})$$

B.2 Existence of Vainshtein-Yukawa branch

So far, we have studied analytic solutions on two different scales. For large radii, $r \gg r_V$, the gravitational potential is a combination of the $1/r$ -law and a Yukawa-type potential:

$$\nu_g = -\frac{r_S}{(1 + \bar{\alpha}^2)} \left(\frac{1}{r} + \frac{4\bar{\alpha}^2}{3} \frac{e^{-m_{\text{FP}} r}}{r} \right) \quad (\text{B.24})$$

as follows from eqs. (B.13) and (B.23). On smaller length scales, $r_S \ll r \ll r_V$ the Stückelberg field μ is nonlinear. The nonlinearities are such that the gravitational potential is given by

$$\nu_g = -\frac{r_S}{r} \quad (\text{B.25})$$

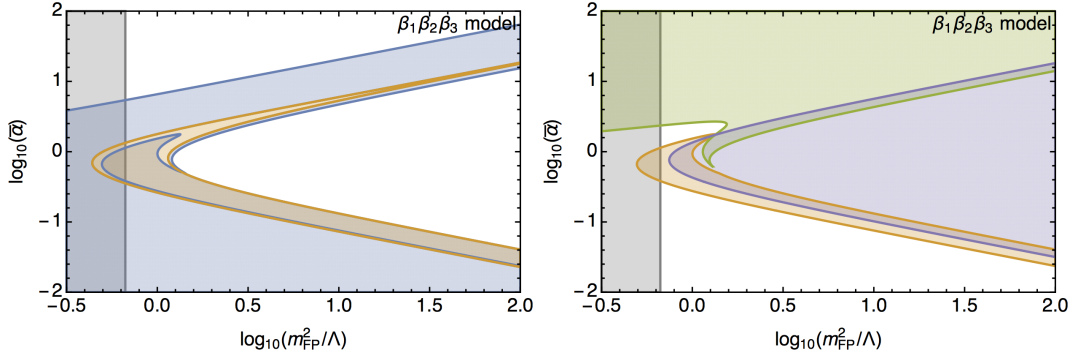


Figure 13. Exclusion plots for a working Vainshtein mechanism for the $\beta_1\beta_2\beta_3$ -model. *Left panel:* In the blue-shaded region $\beta < d_1/d_2$ is implied while in the yellow-shaded region $d_2 < 0$ holds. In the overlap, there is no everywhere real solution for the Stückelberg field μ that incorporates the Vainshtein mechanism at small radii while giving rise to the correct asymptotics. *Right panel:* In the green-shaded region $\mu \ll 1$ is no solution for large radii while in the purple-shaded region $\gamma < 1$. The yellow-shaded region shows the overlap of the bounds presented in the left panel. In the gray shaded region the Higuchi bound is violated. In summary, only outside the shaded regions, the bimetric model incorporates a working Vainshtein mechanism.

as follows from eq. (B.16) on a solution where μ is constant. This is summarised in eq. (4.4). For the screening mechanism to work it is necessary that the solution of the Stückelberg field realising these two regimes exists and is real-valued for every r without branch cuts.

This point was studied in detail in [90]. Firstly, the nonlinear equation (B.19) determining μ must give rise to a solution with $\mu \ll 1$ for $r \gg r_V$, which matches the linearised solution. This is the case only if

$$\beta < \sqrt{\gamma} \quad (\text{B.26})$$

is satisfied. This bound is stated in eq. (4.6) and ensures a consistent asymptotic behavior of the nonlinear solutions. This is the condition ensuring consistent asymptotics as stated in eq. (4.6). Secondly, the linearised solution can be smoothly connected only to the nonlinear solution with $\mu = -1/\sqrt{\gamma}$, which is required to be larger than the solution with $\mu = -1$. Therefore, a consistent screening regime requires the parameters to satisfy

$$\gamma > 1 \quad (\text{B.27})$$

as stated in eq. (4.5). Thirdly, there must be a solution that is real-valued for every r and interpolates between the two aforementioned asymptotic limits without branch cuts. This is the case if the parameters satisfy the following bound:

$$\beta > \frac{d_1}{d_2} \quad \text{if} \quad d_2 < 0, \quad (\text{B.28})$$

where

$$\begin{aligned} d_1 &= -1 + 6(1 + \bar{\alpha}^2)\sqrt{\gamma}(1 + \gamma) - (13 + 12\bar{\alpha}^2)\gamma, \\ d_2 &= 1 + 3\bar{\alpha}^2 - 6(1 + \bar{\alpha}^2)\sqrt{\gamma} + 3(1 + \bar{\alpha}^2)\gamma. \end{aligned} \quad (\text{B.29})$$

The bound in eq. (B.27) implies $\beta_3 > 0$. Combining eqs. (B.26) and (B.27) then implies $\beta_2 < 0$. A theoretically consistent expansion history requires $\beta_1 > 0$. Therefore, the $\beta_1\beta_2\beta_3$ -model is the only bimetric model with up to three free parameters that allows for Vainshtein screening and has a consistent background cosmology. In fig. 13 the bounds in eqs. (B.26) to (B.28) are presented in terms of the physical parameters $\bar{\alpha}$ and m_{FP}^2/Λ for that model. To express the interaction in terms of the physical parameters, we use the parameter relations reported in appendix A. In the left panel the violation of the bound (B.28) is shown. In the overlap of the blue- and yellow-shaded regions, the

Vainshtein-Yukawa solution does not exist. In the right panel, we combine this bound with the other two. The shaded regions represent, where the bounds are violated and hence where the Vainshtein screening mechanism does not work. Only the region left white gives rise to screening. In fig. 7, the Vainshtein bounds are combined with the bounds ensuring a consistent background cosmology.

References

- [1] LIGO SCIENTIFIC, VIRGO collaboration, *Observation of Gravitational Waves from a Binary Black Hole Merger*, *Phys. Rev. Lett.* **116** (2016) 061102 [[1602.03837](#)].
- [2] A. Einstein, *Über Gravitationswellen*, *Sitzungsber. Preuss. Akad. Wiss. Berlin (Math. Phys.)* **1918** (1918) 154.
- [3] LIGO SCIENTIFIC, VIRGO collaboration, *GW170817: Observation of Gravitational Waves from a Binary Neutron Star Inspiral*, *Phys. Rev. Lett.* **119** (2017) 161101 [[1710.05832](#)].
- [4] LIGO SCIENTIFIC, VIRGO, FERMI-GBM, INTEGRAL collaboration, *Gravitational Waves and Gamma-rays from a Binary Neutron Star Merger: GW170817 and GRB 170817A*, *Astrophys. J. Lett.* **848** (2017) L13 [[1710.05834](#)].
- [5] PLANCK collaboration, *Planck 2018 results. VI. Cosmological parameters*, *Astron. Astrophys.* **641** (2020) A6 [[1807.06209](#)].
- [6] ACT collaboration, *The Atacama Cosmology Telescope: DR4 Maps and Cosmological Parameters*, [2007.07288](#).
- [7] K.C. Wong et al., *H0LiCOW – XIII. A 2.4 per cent measurement of H0 from lensed quasars: 5.3 σ tension between early- and late-Universe probes*, *Mon. Not. Roy. Astron. Soc.* **498** (2020) 1420 [[1907.04869](#)].
- [8] A.G. Riess, S. Casertano, W. Yuan, L.M. Macri and D. Scolnic, *Large Magellanic Cloud Cepheid Standards Provide a 1% Foundation for the Determination of the Hubble Constant and Stronger Evidence for Physics beyond Λ CDM*, *Astrophys. J.* **876** (2019) 85 [[1903.07603](#)].
- [9] W.L. Freedman, B.F. Madore, T. Hoyt, I.S. Jang, R. Beaton, M.G. Lee et al., *Calibration of the Tip of the Red Giant Branch (TRGB)*, [2002.01550](#).
- [10] D. Pesce et al., *The Megamaser Cosmology Project. XIII. Combined Hubble constant constraints*, *Astrophys. J. Lett.* **891** (2020) L1 [[2001.09213](#)].
- [11] J.L. Bernal, L. Verde and A.G. Riess, *The trouble with H₀*, *JCAP* **10** (2016) 019 [[1607.05617](#)].
- [12] S. Weinberg, *The Cosmological Constant Problem*, *Rev. Mod. Phys.* **61** (1989) 1.
- [13] J. Martin, *Everything You Always Wanted To Know About The Cosmological Constant Problem (But Were Afraid To Ask)*, *Comptes Rendus Physique* **13** (2012) 566 [[1205.3365](#)].
- [14] G. Dvali and C. Gomez, *Quantum Compositeness of Gravity: Black Holes, AdS and Inflation*, *JCAP* **01** (2014) 023 [[1312.4795](#)].
- [15] G. Dvali and C. Gomez, *Quantum Exclusion of Positive Cosmological Constant?*, *Annalen Phys.* **528** (2016) 68 [[1412.8077](#)].
- [16] G. Dvali, C. Gomez and S. Zell, *Quantum Break-Time of de Sitter*, *JCAP* **06** (2017) 028 [[1701.08776](#)].
- [17] G. Dvali and C. Gomez, *On Exclusion of Positive Cosmological Constant*, *Fortsch. Phys.* **67** (2019) 1800092 [[1806.10877](#)].
- [18] Y. Akrami, R. Kallosh, A. Linde and V. Vardanyan, *The Landscape, the Swampland and the Era of Precision Cosmology*, *Fortsch. Phys.* **67** (2019) 1800075 [[1808.09440](#)].
- [19] G. Obied, H. Ooguri, L. Spodyneiko and C. Vafa, *De Sitter Space and the Swampland*, [1806.08362](#).
- [20] P. Agrawal, G. Obied, P.J. Steinhardt and C. Vafa, *On the Cosmological Implications of the String Swampland*, *Phys. Lett. B* **784** (2018) 271 [[1806.09718](#)].
- [21] S.K. Garg and C. Krishnan, *Bounds on Slow Roll and the de Sitter Swampland*, *JHEP* **11** (2019) 075 [[1807.05193](#)].

- [22] H. Ooguri, E. Palti, G. Shiu and C. Vafa, *Distance and de Sitter Conjectures on the Swampland*, *Phys. Lett. B* **788** (2019) 180 [[1810.05506](#)].
- [23] A. Joyce, L. Lombriser and F. Schmidt, *Dark Energy Versus Modified Gravity*, *Ann. Rev. Nucl. Part. Sci.* **66** (2016) 95 [[1601.06133](#)].
- [24] D. Lovelock, *The Einstein tensor and its generalizations*, *J. Math. Phys.* **12** (1971) 498.
- [25] G.W. Horndeski, *Second-order scalar-tensor field equations in a four-dimensional space*, *Int.J.Theor.Phys.* **10** (1974) 363.
- [26] C. Deffayet, G. Esposito-Farese and A. Vikman, *Covariant Galileon*, *Phys. Rev. D* **79** (2009) 084003 [[0901.1314](#)].
- [27] G. Tasinato, *Cosmic Acceleration from Abelian Symmetry Breaking*, *JHEP* **04** (2014) 067 [[1402.6450](#)].
- [28] L. Heisenberg, *Generalization of the Proca Action*, *JCAP* **05** (2014) 015 [[1402.7026](#)].
- [29] P. Creminelli and F. Vernizzi, *Dark Energy after GW170817 and GRB170817A*, *Phys. Rev. Lett.* **119** (2017) 251302 [[1710.05877](#)].
- [30] J. Sakstein and B. Jain, *Implications of the Neutron Star Merger GW170817 for Cosmological Scalar-Tensor Theories*, *Phys. Rev. Lett.* **119** (2017) 251303 [[1710.05893](#)].
- [31] J.M. Ezquiaga and M. Zumalacárregui, *Dark Energy After GW170817: Dead Ends and the Road Ahead*, *Phys. Rev. Lett.* **119** (2017) 251304 [[1710.05901](#)].
- [32] T. Baker, E. Bellini, P. Ferreira, M. Lagos, J. Noller and I. Sawicki, *Strong constraints on cosmological gravity from GW170817 and GRB 170817A*, *Phys. Rev. Lett.* **119** (2017) 251301 [[1710.06394](#)].
- [33] C. de Rham, G. Gabadadze and A.J. Tolley, *Resummation of Massive Gravity*, *Phys.Rev.Lett.* **106** (2011) 231101 [[1011.1232](#)].
- [34] S. Hassan and R.A. Rosen, *Resolving the Ghost Problem in non-Linear Massive Gravity*, *Phys.Rev.Lett.* **108** (2012) 041101 [[1106.3344](#)].
- [35] C. de Rham, J.T. Deskins, A.J. Tolley and S.-Y. Zhou, *Graviton Mass Bounds*, *Rev. Mod. Phys.* **89** (2017) 025004 [[1606.08462](#)].
- [36] S. Hassan and R.A. Rosen, *Bimetric Gravity from Ghost-free Massive Gravity*, *JHEP* **1202** (2012) 126 [[1109.3515](#)].
- [37] K. Max, M. Platscher and J. Smirnov, *Gravitational Wave Oscillations in Bigravity*, *Phys. Rev. Lett.* **119** (2017) 111101 [[1703.07785](#)].
- [38] K. Max, M. Platscher and J. Smirnov, *Decoherence of Gravitational Wave Oscillations in Bigravity*, *Phys. Rev. D* **97** (2018) 064009 [[1712.06601](#)].
- [39] M. Fierz and W. Pauli, *On relativistic wave equations for particles of arbitrary spin in an electromagnetic field*, *Proc.Roy.Soc.Lond.* **A173** (1939) 211.
- [40] V. Zakharov, *Linearized gravitation theory and the graviton mass*, *JETP Lett.* **12** (1970) 312.
- [41] H. van Dam and M. Veltman, *Massive and massless Yang-Mills and gravitational fields*, *Nucl.Phys.* **B22** (1970) 397.
- [42] A. Vainshtein, *To the problem of nonvanishing gravitation mass*, *Phys.Lett.* **B39** (1972) 393.
- [43] M. Ostrogradsky, *Mémoires sur les équations différentielles, relatives au problème des isopérimètres*, *Mem. Acad. St. Petersbourg* **6** (1850) 385.
- [44] A. Pais and G. Uhlenbeck, *On Field theories with nonlocalized action*, *Phys. Rev.* **79** (1950) 145.
- [45] D. Boulware and S. Deser, *Can gravitation have a finite range?*, *Phys.Rev.* **D6** (1972) 3368.
- [46] C. de Rham and G. Gabadadze, *Generalization of the Fierz-Pauli Action*, *Phys.Rev.* **D82** (2010) 044020 [[1007.0443](#)].
- [47] C. de Rham, G. Gabadadze and A.J. Tolley, *Ghost free Massive Gravity in the Stückelberg language*, *Phys.Lett.* **B711** (2012) 190 [[1107.3820](#)].
- [48] S. Hassan, R.A. Rosen and A. Schmidt-May, *Ghost-free Massive Gravity with a General Reference Metric*, *JHEP* **1202** (2012) 026 [[1109.3230](#)].

- [49] S. Hassan and R.A. Rosen, *Confirmation of the Secondary Constraint and Absence of Ghost in Massive Gravity and Bimetric Gravity*, *JHEP* **1204** (2012) 123 [[1111.2070](#)].
- [50] S. Hassan, A. Schmidt-May and M. von Strauss, *Proof of Consistency of Nonlinear Massive Gravity in the Stückelberg Formulation*, *Phys.Lett.* **B715** (2012) 335 [[1203.5283](#)].
- [51] S. Hassan and A. Lundkvist, *Analysis of constraints and their algebra in bimetric theory*, *JHEP* **08** (2018) 182 [[1802.07267](#)].
- [52] V. Errasti Díez, M. Maier, J.A. Méndez-Zavaleta and M. Taslimi Tehrani, *Lagrangian constraint analysis of first-order classical field theories with an application to gravity*, *Phys. Rev. D* **102** (2020) 065015 [[2007.11020](#)].
- [53] G. D'Amico, C. de Rham, S. Dubovsky, G. Gabadadze, D. Pirtskhalava and A.J. Tolley, *Massive Cosmologies*, *Phys. Rev.* **D84** (2011) 124046 [[1108.5231](#)].
- [54] A.E. Gümrükçüoğlu, C. Lin and S. Mukohyama, *Open FRW universes and self-acceleration from nonlinear massive gravity*, *JCAP* **1111** (2011) 030 [[1109.3845](#)].
- [55] A.E. Gümrükçüoğlu, C. Lin and S. Mukohyama, *Cosmological perturbations of self-accelerating universe in nonlinear massive gravity*, *JCAP* **1203** (2012) 006 [[1111.4107](#)].
- [56] A. De Felice, A.E. Gümrükçüoğlu and S. Mukohyama, *Massive gravity: nonlinear instability of the homogeneous and isotropic universe*, *Phys.Rev.Lett.* **109** (2012) 171101 [[1206.2080](#)].
- [57] K. Hinterbichler, *Theoretical Aspects of Massive Gravity*, *Rev.Mod.Phys.* **84** (2012) 671 [[1105.3735](#)].
- [58] C. de Rham, *Massive Gravity*, *Living Rev.Rel.* **17** (2014) 7 [[1401.4173](#)].
- [59] M.S. Volkov, *Cosmological solutions with massive gravitons in the bigravity theory*, *JHEP* **1201** (2012) 035 [[1110.6153](#)].
- [60] M. von Strauss, A. Schmidt-May, J. Enander, E. Mörtzell and S. Hassan, *Cosmological Solutions in Bimetric Gravity and their Observational Tests*, *JCAP* **1203** (2012) 042 [[1111.1655](#)].
- [61] D. Comelli, M. Crisostomi, F. Nesti and L. Pilo, *FRW Cosmology in Ghost Free Massive Gravity*, *JHEP* **1203** (2012) 067 [[1111.1983](#)].
- [62] M.S. Volkov, *Exact self-accelerating cosmologies in the ghost-free bigravity and massive gravity*, *Phys.Rev.* **D86** (2012) 061502 [[1205.5713](#)].
- [63] M.S. Volkov, *Exact self-accelerating cosmologies in the ghost-free massive gravity – the detailed derivation*, *Phys.Rev.* **D86** (2012) 104022 [[1207.3723](#)].
- [64] Y. Akrami, T.S. Koivisto and M. Sandstad, *Accelerated expansion from ghost-free bigravity: a statistical analysis with improved generality*, *JHEP* **1303** (2013) 099 [[1209.0457](#)].
- [65] A. De Felice, A.E. Gümrükçüoğlu, S. Mukohyama, N. Tanahashi and T. Tanaka, *Viable cosmology in bimetric theory*, *JCAP* **1406** (2014) 037 [[1404.0008](#)].
- [66] M.S. Volkov, *Self-accelerating cosmologies and hairy black holes in ghost-free bigravity and massive gravity*, *Class.Quant.Grav.* **30** (2013) 184009 [[1304.0238](#)].
- [67] F. Könnig, A. Patil and L. Amendola, *Viable cosmological solutions in massive bimetric gravity*, *JCAP* **1403** (2014) 029 [[1312.3208](#)].
- [68] E. Mörtzell and S. Dhawan, *Does the Hubble constant tension call for new physics?*, *JCAP* **1809** (2018) 025 [[1801.07260](#)].
- [69] M. Lüben, A. Schmidt-May and J. Smirnov, *Vainshtein Screening in Bimetric Cosmology*, *Phys. Rev. D* **102** (2020) 123529 [[1912.09449](#)].
- [70] D. Comelli, M. Crisostomi and L. Pilo, *Perturbations in Massive Gravity Cosmology*, *JHEP* **1206** (2012) 085 [[1202.1986](#)].
- [71] N. Khosravi, H.R. Sepangi and S. Shahidi, *Massive cosmological scalar perturbations*, *Phys. Rev. D* **86** (2012) 043517 [[1202.2767](#)].
- [72] M. Berg, I. Buchberger, J. Enander, E. Mörtzell and S. Sjörs, *Growth Histories in Bimetric Massive Gravity*, *JCAP* **1212** (2012) 021 [[1206.3496](#)].

- [73] Y. Sakakihara, J. Soda and T. Takahashi, *On Cosmic No-hair in Bimetric Gravity and the Higuchi Bound*, *PTEP* **2013** (2013) 033E02 [[1211.5976](#)].
- [74] F. Könnig and L. Amendola, *Instability in a minimal bimetric gravity model*, *Phys.Rev.* **D90** (2014) 044030 [[1402.1988](#)].
- [75] D. Comelli, M. Crisostomi and L. Pilo, *FRW Cosmological Perturbations in Massive Bigravity*, *Phys.Rev.* **D90** (2014) 084003 [[1403.5679](#)].
- [76] A.R. Solomon, Y. Akrami and T.S. Koivisto, *Linear growth of structure in massive bigravity*, *JCAP* **1410** (2014) 066 [[1404.4061](#)].
- [77] F. Könnig, Y. Akrami, L. Amendola, M. Motta and A.R. Solomon, *Stable and unstable cosmological models in bimetric massive gravity*, *Phys.Rev.* **D90** (2014) 124014 [[1407.4331](#)].
- [78] M. Lagos and P.G. Ferreira, *Cosmological perturbations in massive bigravity*, *JCAP* **1412** (2014) 026 [[1410.0207](#)].
- [79] F. Könnig, *Higuchi Ghosts and Gradient Instabilities in Bimetric Gravity*, *Phys.Rev.* **D91** (2015) 104019 [[1503.07436](#)].
- [80] Y. Akrami, S.F. Hassan, F. Könnig, A. Schmidt-May and A.R. Solomon, *Bimetric gravity is cosmologically viable*, *Phys. Lett.* **B748** (2015) 37 [[1503.07521](#)].
- [81] K. Aoki, K.-i. Maeda and R. Namba, *Stability of the Early Universe in Bigravity Theory*, *Phys. Rev.* **D92** (2015) 044054 [[1506.04543](#)].
- [82] E. Mörtzell and J. Enander, *Scalar instabilities in bimetric gravity: The Vainshtein mechanism and structure formation*, *JCAP* **1510** (2015) 044 [[1506.04977](#)].
- [83] K. Aoki and S. Mukohyama, *Massive gravitons as dark matter and gravitational waves*, *Phys. Rev. D* **94** (2016) 024001 [[1604.06704](#)].
- [84] E. Babichev, L. Marzola, M. Raidal, A. Schmidt-May, F. Urban, H. Veermaäe et al., *Bigravitational origin of dark matter*, *Phys. Rev.* **D94** (2016) 084055 [[1604.08564](#)].
- [85] E. Babichev, L. Marzola, M. Raidal, A. Schmidt-May, F. Urban, H. Veermäe et al., *Heavy spin-2 Dark Matter*, *JCAP* **1609** (2016) 016 [[1607.03497](#)].
- [86] X. Chu and C. Garcia-Cely, *Self-interacting Spin-2 Dark Matter*, *Phys. Rev.* **D96** (2017) 103519 [[1708.06764](#)].
- [87] D. Comelli, M. Crisostomi, F. Nesti and L. Pilo, *Spherically Symmetric Solutions in Ghost-Free Massive Gravity*, *Phys.Rev.* **D85** (2012) 024044 [[1110.4967](#)].
- [88] M. Platscher, J. Smirnov, S. Meyer and M. Bartelmann, *Long Range Effects in Gravity Theories with Vainshtein Screening*, *JCAP* **1812** (2018) 009 [[1809.05318](#)].
- [89] J. Enander and E. Mörtzell, *Strong lensing constraints on bimetric massive gravity*, *JHEP* **1310** (2013) 031 [[1306.1086](#)].
- [90] J. Enander and E. Mörtzell, *On stars, galaxies and black holes in massive bigravity*, *JCAP* **1511** (2015) 023 [[1507.00912](#)].
- [91] M. Hohmann, *Post-Newtonian parameter γ and the deflection of light in ghost-free massive bimetric gravity*, *Phys. Rev. D* **95** (2017) 124049 [[1701.07700](#)].
- [92] M. Lüben, E. Mörtzell and A. Schmidt-May, *Bimetric cosmology is compatible with local tests of gravity*, *Class. Quant. Grav.* **37** (2020) 047001 [[1812.08686](#)].
- [93] E. Babichev and M. Crisostomi, *Restoring general relativity in massive bigravity theory*, *Phys. Rev.* **D88** (2013) 084002 [[1307.3640](#)].
- [94] A. De Felice, T. Nakamura and T. Tanaka, *Possible existence of viable models of bi-gravity with detectable graviton oscillations by gravitational wave detectors*, *PTEP* **2014** (2014) 043E01 [[1304.3920](#)].
- [95] G. Cusin, R. Durrer, P. Guarato and M. Motta, *Gravitational waves in bigravity cosmology*, *JCAP* **05** (2015) 030 [[1412.5979](#)].

- [96] L. Amendola, F. König, M. Martinelli, V. Pettorino and M. Zumalacárregui, *Surfing gravitational waves: can bigravity survive growing tensor modes?*, *JCAP* **05** (2015) 052 [[1503.02490](#)].
- [97] M. Johnson and A. Terrana, *Tensor Modes in Bigravity: Primordial to Present*, *Phys. Rev. D* **92** (2015) 044001 [[1503.05560](#)].
- [98] Y. Sakakihara and J. Soda, *Primordial Gravitational Waves in Bimetric Gravity*, *JCAP* **09** (2015) 015 [[1504.04969](#)].
- [99] M. Fasiello and R.H. Ribeiro, *Mild bounds on bigravity from primordial gravitational waves*, *JCAP* **07** (2015) 027 [[1505.00404](#)].
- [100] G. Cusin, R. Durrer, P. Guarato and M. Motta, *Inflationary perturbations in bimetric gravity*, *JCAP* **09** (2015) 043 [[1505.01091](#)].
- [101] Y. Sakakihara and T. Tanaka, *Primordial fluctuations from inflation in dRGT bimetric theory of gravity*, *JCAP* **09** (2016) 033 [[1605.05790](#)].
- [102] M. Biagetti, E. Dimastrogiovanni and M. Fasiello, *Possible signatures of the inflationary particle content: spin-2 fields*, *JCAP* **10** (2017) 038 [[1708.01587](#)].
- [103] E. Dimastrogiovanni, M. Fasiello and G. Tasinato, *Probing the inflationary particle content: extra spin-2 field*, *JCAP* **08** (2018) 016 [[1806.00850](#)].
- [104] J.B. Jiménez, J.M. Ezquiaga and L. Heisenberg, *Probing cosmological fields with gravitational wave oscillations*, *JCAP* **04** (2020) 027 [[1912.06104](#)].
- [105] M. Lüben, A. Schmidt-May and J. Weller, *Physical parameter space of bimetric theory and SN1a constraints*, *JCAP* **09** (2020) 024 [[2003.03382](#)].
- [106] S. Dhawan, A. Goobar, E. Mörtzell, R. Amanullah and U. Feindt, *Narrowing down the possible explanations of cosmic acceleration with geometric probes*, *JCAP* **07** (2017) 040 [[1705.05768](#)].
- [107] M. Lindner, K. Max, M. Platscher and J. Rezacek, *Probing alternative cosmologies through the inverse distance ladder*, *JCAP* **10** (2020) 040 [[2002.01487](#)].
- [108] E. Fischbach and C. Talmadge, *The Search for Non-Newtonian Gravity*, Springer-Verlag New York (1999), [10.1007/978-1-4612-1438-0](#).
- [109] E. Adelberger, B.R. Heckel and A. Nelson, *Tests of the gravitational inverse square law*, *Ann. Rev. Nucl. Part. Sci.* **53** (2003) 77 [[hep-ph/0307284](#)].
- [110] E. Adelberger, J. Gundlach, B. Heckel, S. Hoedl and S. Schlamminger, *Torsion balance experiments: A low-energy frontier of particle physics*, *Prog. Part. Nucl. Phys.* **62** (2009) 102.
- [111] J. Murata and S. Tanaka, *A review of short-range gravity experiments in the LHC era*, *Class. Quant. Grav.* **32** (2015) 033001 [[1408.3588](#)].
- [112] B. Bertotti, L. Iess and P. Tortora, *A test of general relativity using radio links with the Cassini spacecraft*, *Nature* **425** (2003) 374.
- [113] C.M. Will, *The Confrontation between General Relativity and Experiment*, *Living Rev. Rel.* **17** (2014) 4 [[1403.7377](#)].
- [114] A. Schmidt-May and M. von Strauss, *Recent developments in bimetric theory*, *J. Phys.* **A49** (2016) 183001 [[1512.00021](#)].
- [115] S. Hassan and R.A. Rosen, *On Non-Linear Actions for Massive Gravity*, *JHEP* **1107** (2011) 009 [[1103.6055](#)].
- [116] S. Hassan and M. Kocic, *On the local structure of spacetime in ghost-free bimetric theory and massive gravity*, *JHEP* **05** (2018) 099 [[1706.07806](#)].
- [117] C. de Rham, L. Heisenberg and R.H. Ribeiro, *On couplings to matter in massive (bi-)gravity*, *Class. Quant. Grav.* **32** (2015) 035022 [[1408.1678](#)].
- [118] C. de Rham, L. Heisenberg and R.H. Ribeiro, *Ghosts & Matter Couplings in Massive (bi- & multi-)Gravity*, *Phys. Rev.* **D90** (2014) 124042 [[1409.3834](#)].
- [119] L. Heisenberg, *Quantum corrections in massive bigravity and new effective composite metrics*, *Class. Quant. Grav.* **32** (2015) 105011 [[1410.4239](#)].

- [120] L. Heisenberg, *More on effective composite metrics*, *Phys. Rev.* **D92** (2015) 023525 [[1505.02966](#)].
- [121] K. Hinterbichler and R.A. Rosen, *Note on ghost-free matter couplings in massive gravity and multigravity*, *Phys. Rev.* **D92** (2015) 024030 [[1503.06796](#)].
- [122] M. Lüben and A. Schmidt-May, *Ghost-Free Completion of An Effective Matter Coupling in Bimetric Theory*, *Fortsch. Phys.* **66** (2018) 1800031 [[1804.04671](#)].
- [123] S. Hassan, A. Schmidt-May and M. von Strauss, *On Consistent Theories of Massive Spin-2 Fields Coupled to Gravity*, *JHEP* **1305** (2013) 086 [[1208.1515](#)].
- [124] H. Nersisyan, Y. Akrami and L. Amendola, *Consistent metric combinations in cosmology of massive bigravity*, *Phys. Rev.* **D92** (2015) 104034 [[1502.03988](#)].
- [125] G. Cusin, R. Durrer, P. Guarato and M. Motta, *A general mass term for bigravity*, *JCAP* **1604** (2016) 051 [[1512.02131](#)].
- [126] M. Fasiello and A.J. Tolley, *Cosmological Stability Bound in Massive Gravity and Bigravity*, *JCAP* **1312** (2013) 002 [[1308.1647](#)].
- [127] A. Higuchi, *Forbidden Mass Range for Spin-2 Field Theory in De Sitter Space-time*, *Nucl.Phys.* **B282** (1987) 397.
- [128] M. Höggås, F. Torsello and E. Mörtzell, *On the Stability of Bimetric Structure Formation*, Submitted to: *JCAP* (2019) [[1910.01651](#)].
- [129] L. Chen, Q.-G. Huang and K. Wang, *Distance priors from planck final release*, *Journal of Cosmology and Astroparticle Physics* **2019** (2019) 028?028.
- [130] SDSS collaboration, *Improved cosmological constraints from a joint analysis of the SDSS-II and SNLS supernova samples*, *Astron. Astrophys.* **568** (2014) A22 [[1401.4064](#)].
- [131] WMAP collaboration, *Five-Year Wilkinson Microwave Anisotropy Probe (WMAP) Observations: Cosmological Interpretation*, *Astrophys. J. Suppl.* **180** (2009) 330 [[0803.0547](#)].
- [132] Z. Zhai, C.-G. Park, Y. Wang and B. Ratra, *Cmb distance priors revisited: effects of dark energy dynamics, spatial curvature, primordial power spectrum, and neutrino parameters*, *Journal of Cosmology and Astroparticle Physics* **2020** (2020) 009?009.
- [133] W. Hu and N. Sugiyama, *Small scale cosmological perturbations: An Analytic approach*, *Astrophys. J.* **471** (1996) 542 [[astro-ph/9510117](#)].
- [134] F. Beutler, C. Blake, M. Colless, D.H. Jones, L. Staveley-Smith, L. Campbell et al., *The 6df galaxy survey: baryon acoustic oscillations and the local hubble constant*, *Monthly Notices of the Royal Astronomical Society* **416** (2011) 3017?3032.
- [135] A.J. Ross, L. Samushia, C. Howlett, W.J. Percival, A. Burden and M. Manera, *The clustering of the sdss dr7 main galaxy sample ? i. a 4 per cent distance measure at redshift 0.15*, *Monthly Notices of the Royal Astronomical Society* **449** (2015) 835?847.
- [136] S. Alam, M. Ata, S. Bailey, F. Beutler, D. Bizyaev, J.A. Blazek et al., *The clustering of galaxies in the completed sdss-iii baryon oscillation spectroscopic survey: cosmological analysis of the dr12 galaxy sample*, *Monthly Notices of the Royal Astronomical Society* **470** (2017) 2617?2652.
- [137] J.E. Bautista, M. Vargas-Magaña, K.S. Dawson, W.J. Percival, J. Brinkmann, J. Brownstein et al., *The sdss-iv extended baryon oscillation spectroscopic survey: Baryon acoustic oscillations at redshift of 0.72 with the dr14 luminous red galaxy sample*, *The Astrophysical Journal* **863** (2018) 110.
- [138] G.-B. Zhao, Y. Wang, S. Saito, H. Gil-Marín, W.J. Percival, D. Wang et al., *The clustering of the sdss-iv extended baryon oscillation spectroscopic survey dr14 quasar sample: a tomographic measurement of cosmic structure growth and expansion rate based on optimal redshift weights*, *Monthly Notices of the Royal Astronomical Society* **482** (2018) 3497?3513.
- [139] G. Schwarz, *Estimating the Dimension of a Model*, *Annals Statist.* **6** (1978) 461.
- [140] R.E. Kass and A.E. Raftery, *Bayes Factors*, *J. Am. Statist. Assoc.* **90** (1995) 773.
- [141] E. Aubourg et al., *Cosmological implications of baryon acoustic oscillation measurements*, *Phys. Rev. D* **92** (2015) 123516 [[1411.1074](#)].

- [142] E. Di Valentino, *A (brave) combined analysis of the H_0 late time direct measurements and the impact on the Dark Energy sector*, [2011.00246](#).
- [143] J. Hoskins, R. Newman, R. Spero and J. Schultz, *Experimental tests of the gravitational inverse square law for mass separations from 2-cm to 105-cm*, *Phys. Rev. D* **32** (1985) 3084.
- [144] R. Spero, J. Hoskins, R. Newman, J. Pellam and J. Schultz, *Test of the Gravitational Inverse-Square Law at Laboratory Distances*, *Phys. Rev. Lett.* **44** (1980) 1645.
- [145] C.D. Hoyle, D.J. Kapner, B.R. Heckel, E.G. Adelberger, J.H. Gundlach, U. Schmidt et al., *Sub-millimeter tests of the gravitational inverse-square law*, *Phys. Rev.* **D70** (2004) 042004 [[hep-ph/0405262](#)].
- [146] S. Smullin, A. Geraci, D. Weld, J. Chiaverini, S.P. Holmes and A. Kapitulnik, *New constraints on Yukawa-type deviations from Newtonian gravity at 20 microns*, *Phys. Rev. D* **72** (2005) 122001 [[hep-ph/0508204](#)].
- [147] A. Cornaz, B. Hubler and W. Kuendig, *Determination of the gravitational constant at an effective interaction distance of 112-m*, *Phys. Rev. Lett.* **72** (1994) 1152.
- [148] B. Hubler, A. Cornaz and W. Kuendig, *Determination of the gravitational constant with a lake experiment: New constraints for non-Newtonian gravity*, *Phys. Rev. D* **51** (1995) 4005.
- [149] J. Thomas, P. Kasameyer, O. Fackler, D. Felske, R. Harris, J. Kammeraad et al., *Testing the inverse-square law of gravity on a 465-m tower*, *Phys. Rev. Lett.* **63** (1989) 1902.
- [150] J. Kammeraad, P. Kasameyer, O. Fackler, D. Felske, R. Harris, M. Millett et al., *New results from Nevada: A Test of Newton's law using the BREN tower and a high density ground gravity survey*, in *10th Moriond Workshop: New and Exotic Phenomena*, pp. 245–254, 1990.
- [151] A.J. Romaides, R.W. Sands, E. Fischbach and C.L. Talmadge, *Final results from the WABG tower gravity experiment*, *Phys. Rev. D* **55** (1997) 4532.
- [152] D.E. Smith, D.C. Christodoulidis, R. Kolenkiewicz, P.J. Dunn, S.M. Klosko, M.H. Torrence et al., *A global geodetic reference frame from LAGEOS ranging (SL5.1AP)*, *Journal of Geophysical Research: Solid Earth* **90** (1985) 9221.
- [153] R.H. Rapp, *An estimate of equatorial gravity from terrestrial and satellite data*, *Geophysical Research Letters* **14** (1987) 730.
- [154] J. Dickey et al., *Lunar Laser Ranging: A Continuing Legacy of the Apollo Program*, *Science* **265** (1994) 482.
- [155] C. Talmadge, J. Berthias, R. Hellings and E. Standish, *Model Independent Constraints on Possible Modifications of Newtonian Gravity*, *Phys. Rev. Lett.* **61** (1988) 1159.
- [156] E. Babichev, C. Deffayet and R. Ziour, *Recovering General Relativity from massive gravity*, *Phys. Rev. Lett.* **103** (2009) 201102 [[0907.4103](#)].
- [157] E. Babichev, C. Deffayet and R. Ziour, *The Vainshtein mechanism in the Decoupling Limit of massive gravity*, *JHEP* **05** (2009) 098 [[0901.0393](#)].
- [158] E. Babichev, C. Deffayet and R. Ziour, *The Recovery of General Relativity in massive gravity via the Vainshtein mechanism*, *Phys. Rev. D* **82** (2010) 104008 [[1007.4506](#)].
- [159] E. Babichev and C. Deffayet, *An introduction to the Vainshtein mechanism*, *Class.Quant.Grav.* **30** (2013) 184001 [[1304.7240](#)].
- [160] M.S. Volkov, *Hairy black holes in the ghost-free bigravity theory*, *Phys.Rev.* **D85** (2012) 124043 [[1202.6682](#)].
- [161] T. Hiramatsu, W. Hu, K. Koyama and F. Schmidt, *Equivalence Principle Violation in Vainshtein Screened Two-Body Systems*, *Phys. Rev. D* **87** (2013) 063525 [[1209.3364](#)].
- [162] J.K. Bloomfield, C. Burrage and A.-C. Davis, *Shape dependence of Vainshtein screening*, *Phys. Rev. D* **91** (2015) 083510 [[1408.4759](#)].
- [163] H. Geng and A. Karch, *Massive islands*, *JHEP* **09** (2020) 121 [[2006.02438](#)].

- [164] G. 't Hooft, *Naturalness, chiral symmetry, and spontaneous chiral symmetry breaking*, *NATO Sci. Ser. B* **59** (1980) 135.
- [165] A. Lewis, *GetDist: a Python package for analysing Monte Carlo samples*, [1910.13970](#).
- [166] M. Platscher and J. Smirnov, *Degravitation of the Cosmological Constant in Bigravity*, *JCAP* **03** (2017) 051 [[1611.09385](#)].